was changed to Dulbecco's modified Eagle's medium supplemented with 10% fetal bovine serum (FBS) or 1% FBS and 5 ng/ml TNFα. Finally, 96 hours after transfection, we determined the relative number of viable RASFs, using the Cell Counting Kit-8 assay.

Cloning and expression of human SPACIA1 and preparation of anti-SPACIA1 antibodies. We designed the following polymerase chain reaction (PCR) primers on the basis of the sequence of human *SAAL1*, which is identical to *SPACIA1* (GenBank Refseq NM_138421; http://www.ncbi.nlm.nih.gov/genbank/): for the first PCR, hSPACIA1+ 5′-AAAGTCATGGACCGCAAC-3′, hSPACIA1− 5′-CCAATTCAGGTTTTAAGTCTGAAC-3′; for the second PCR, hSPACIA1+/*Not* I 5′-ATATGCGGCCGCCGATGGACCGCAACCCCTCG-3′, hSPACIA1−/*Xho* I 5′-TCACTCGAGGTTTTAAGTCTGAACCTTC-3′. Human RASF cDNA was used as a template for PCR. The product was cloned into a pcDNA3-FLAG vector, which was constructed by inserting the FLAG sequence into pcDNA3 (Invitrogen). To create a GST-SPACIA1 fusion protein, the *SPACIA1* gene was subcloned into a pGEX-6P vector (GE Healthcare) and then transformed into *Escherichia coli* BL21 cells. The transfected cells were cultured for 4 hours at 30°C in the presence of 0.1 m*M* isopropyl β-D-1-thiogalactopyranoside. Subsequently, the cells were sonicated, and the recombinant human SPACIA1 protein was purified from the lysate with a glutathione Sepharose 4B column (GE Healthcare) and PreScission protease cleavage. Finally, the purified human SPACIA1 protein was used as an antigen to generate polyclonal antibodies and monoclonal antibodies (pAb and mAb, respectively), using standard methods as previously described (10,11).

Western blotting. Synovial fibroblasts from patients with RA and synovial tissue from patients with OA and RA were lysed in lysis buffer (20 m*M* Tris [pH 7.5], 150 m*M* NaCl, 0.5% Nonidet P40, 1 m*M* EDTA, 1 m*M* dithiothreitol, 5 m*M* NaF, 0.2 m*M* Na_3VO_4, and protease inhibitors). Then whole cell lysates (10 μg) or tissue lysates (20 μg) were electrophoresed on 10% sodium dodecyl sulfate polyacrylamide gels and transferred onto activated Immobilon-P polyvinylidene fluoride membranes (Millipore) using a wet transfer method. After blocking with 5% nonfat dry milk in phosphate buffered saline (PBS), the membranes were incubated with anti-human SPACIA1 mAb (clone 1Ac; 1:500 dilution), followed by incubation with horseradish peroxidase (HRP)–labeled anti-mouse IgG antibody (1:20,000 dilution; The Binding Site) for 1 hour at room temperature, and detection with Immobilon Western Chemiluminescent HRP Substrate (Millipore). The signal intensities of the bands specific for SPACIA1 were quantified using ImageJ software (National Institutes of Health; http://rsbweb.nih.gov/ij/). To investigate the expression of SPACIA1 in various human tissues, we used a human multiple tissue blot (Calbiochem). The detection method was the same as described above, except the primary antibody was anti-human SPACIA1 pAb (1:8,000 dilution) and the secondary antibody was HRP-labeled anti-rabbit IgG antibody (1:20,000 dilution).

Immunocytochemistry. To determine the intracellular localization of SPACIA1 in RASFs, we performed immunofluorescence staining as previously described (12). Anti-human SPACIA1 mAb (clone 1Ac) and normal mouse IgG were used as the primary antibody and negative control, respectively. The secondary antibody was a rhodamine-conjugated anti-mouse IgG antibody (Millipore). Nuclei were stained with DAPI.

Immunohistochemistry. Human synovial tissue specimens and mouse knee joints were fixed in 10% formalin and then embedded in paraffin. To retrieve antigens, deparaffinized tissue sections (5 μm thick) were microwaved for 5 minutes and soaked in 1 m*M* EDTA solution (pH 8.0) for 40 minutes at 90°C. After blocking of endogenous peroxidase activity for 10 minutes in 3% methanol, the sections were incubated with anti-human SPACIA1 pAb (1.5 μg/ml), normal rabbit IgG (1.5 μg/ml), anti-CD14 mAb (1:150 dilution; Leica), anti-CD163 mAb (1:150 dilution; Leica), or normal mouse IgG (1 μg/ml) for 30 minutes at room temperature. Subsequently, the sections were rinsed and visualized by immunoperoxidase staining with the Vectastain ABC-PO kit (Vector) and 3,3′-diaminobenzidine tetrahydrochloride substrate. Mayer's hematoxylin was used as a counterstain. Normal rabbit IgG and normal mouse IgG were used as negative controls.

Cell cycle phase analysis. To analyze the effect of *SPACIA1* siRNA on the cell cycle of RASFs, we used *SPACIA1* siRNA and mock siRNA. The target sequences were as follows: human SPACIA1 3′-untranslated region siRNA 5′-GAAUUACUUCUGUACAAGAA-3′, mock siRNA (negative control) 5′-UAAGGCUAUGAAGAGAUAC-3′. Ninety-six hours after transfection of siRNA into RASFs, the cells were harvested, washed, and suspended in PBS with 0.1% Triton X-100. The suspension was filtered through nylon mesh to remove aggregates. Subsequently, RNase and propidium iodide were added to the suspension, which was analyzed on a FACSCalibur flow cytometer (BD Biosciences). The results were analyzed using FlowJo software (Tree Star).

Annexin V–based apoptosis assay. To evaluate apoptotic cells, we used the same siRNAs that were used for the cell cycle analysis and analyzed RASFs 96 hours after transfection. RASFs that were treated with 10 μ*M* staurosporine for 3 hours and cultured for 12 hours were used as a positive control. Staurosporine-treated or siRNA-transfected RASFs were stained with fluorescein isothiocyanate (FITC)–labeled annexin V (MBL) using a previously described immunofluorescence staining procedure (12), and the percentage of annexin V–positive RASFs in 3 microscopic fields (200×) was calculated.

Bromodeoxyuridine (BrdU) incorporation assay. For measurement of BrdU incorporation, we used *SPACIA1* siRNA, negative control siRNA, and *PCNA* siRNA (proliferating cell nuclear antigen) (On-Target plus SMARTpool). RASFs were trypsinized and then seeded on a 6-well plate (1.4×10^5 cells/well). After 18 hours, 33 n*M* siRNA was transfected into the cells with Lipofectamine 2000. Twenty-four hours later, 10 μ*M* aphidicolin was added to the culture media for 24 hours to synchronize the cells at the G_1 phase. Then the aphidicolin was removed and DNA synthesis was determined by measurement of BrdU incorporation for 8 hours. Subsequently, the cells were fixed, permeabilized, treated with DNase I, and stained for 1 hour with an FITC-labeled anti-BrdU antibody (BD Biosciences). Fluorescence intensity was measured with a Cellomics ArrayScan VTI HCS reader (Thermo Fisher Scientific).

Generation of *SPACIA1*-overexpressing mice. On the basis of the sequence of mouse *SAAL1* (GenBank Refseq NM_030233), we designed the following primers: for the first

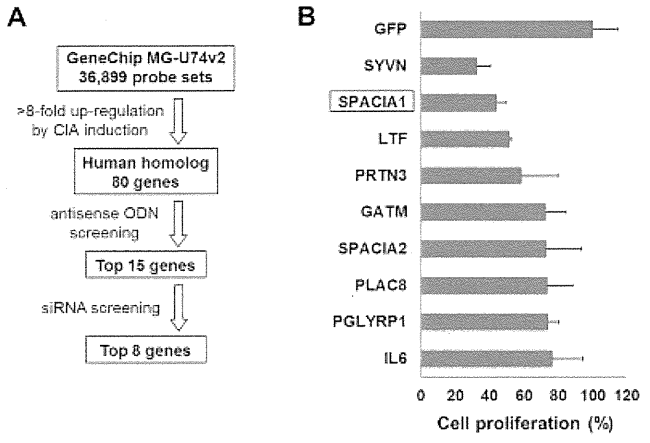

Figure 1. Identification of *SPACIA1* by whole-genome microarray analysis and functional screening. **A**, Flow chart of the procedure that was used to select 8 genes from >36,000 mouse transcripts. Eighty genes were up-regulated >8-fold in the foot joints of mice with collagen-induced arthritis (CIA). Among these genes, 15 genes that inhibited the proliferation of human rheumatoid arthritis synovial fibroblasts (RASFs) were identified with antisense oligodeoxynucleotides (ODNs). Finally, 8 candidate genes were isolated using small interfering RNAs (siRNAs) that were targeted against these 15 genes. **B**, Rate of proliferation of RASFs that were transfected with siRNA targeted against the candidate genes. The results are expressed as the percentage of the proliferation rate of RASFs that were transfected with green fluorescence protein (GFP) siRNA (negative control). Small interfering RNA against synoviolin (*SYVN*), an E3 ubiquitin ligase that we previously identified as a pathogenic factor in arthropathy (7), was used as a positive control. All experiments were performed in triplicate. Values are the mean ± SD.

PCR, mSPACIA1+ 5′-CATCGGCATGGATCGAAAC–3′, mSPACIA1− 5′-ATGCCAACTTCGAACCATAG-3′; for the second PCR, mSPACIA1+/*Mun* I 5′-ATACAATTGATGGATCGAAACCCGTCTC-3′, mSPACIA1−/*Xho* I 5′-TAACTCGAGTTAAGTCTGTGCCTTCAC-3′. PCR was performed with a mouse embryo (17th day of gestation) cDNA as a template. The PCR product was cloned into the pcDNA3-FLAG vector, and the FLAG-tagged mouse *SPACIA1* gene was subcloned into the mammalian expression vector pJC13-1 (a kind gift from Dr. Suming Huang, University of Florida, Gainesville) with a CAG promoter and β-globin insulators (13). The linearized FLAG-tagged mouse SPACIA1 pJC13-1 expression vector was injected into the pronucleus of fertilized eggs from C57BL/6 mice (Macrogen). To confirm the overexpression of mouse *SPACIA1*, genomic DNA and protein were extracted from tails and used for PCR and Western blotting analyses, respectively. Finally, the *SPACIA1*-overexpressing mice were backcrossed onto the DBA/1J strain for 7 generations.

Histopathologic examination. Human synovial tissue specimens were obtained from patients with RA (n = 9) or OA (n = 9) and processed as described previously (14). Synovitis was scored on a 0–3 scale using the grading system of Krenn et al (1).

Mouse knee joints were removed 42 days after CIA induction, fixed in 10% formalin, and embedded in paraffin. Deparaffinized tissue sections (5 μm thick) were stained with hematoxylin and eosin. The sections were scored on a scale of 0–4 under blinded conditions, according to the degree of hyperplasia in the synovial lining, mononuclear cell infiltration, and pannus formation, as described previously (15).

Statistical analysis. Fisher's exact test was used to analyze the correlation between expression levels of SPACIA1 and pathologic features of synovitis. The significance of RASF proliferation was analyzed by one-way analysis of variance and Tukey's post hoc test. The chi-square test (or Fisher's exact test) was used to compare the incidence of arthritis between transgenic and wild-type mice. Arthritis scores and histopathologic scores in transgenic and wild-type mice were compared by Mann-Whitney U test. All other statistical analyses were performed using Student's unpaired *t*-test. *P* values less than 0.05 were considered significant.

RESULTS

Identification of novel genes associated with synoviocyte proliferation. In the transcriptome of the foot joints of mice with CIA, we detected 80 genes (among ~36,000 mRNA probes) that were up-regulated >8-fold compared with those of healthy control mice (Figure 1A). By transfecting human RASFs with antisense ODNs specific for the human homologs of these 80

Figure 2. Amino acid sequence alignment of mouse and human *SPACIA1*. The alignment was generated using the ClustalW2 multiple sequence alignment program (http://www.ebi.ac.uk/Tools/clustalw2/). Identical residues are marked with asterisks. Colons and periods indicate conserved substitutions and semiconserved substitutions, respectively. Shaded regions indicate armadillo repeats (InterPro accession no. IPR016024). Boxed amino acids indicate phosphorylation sites.

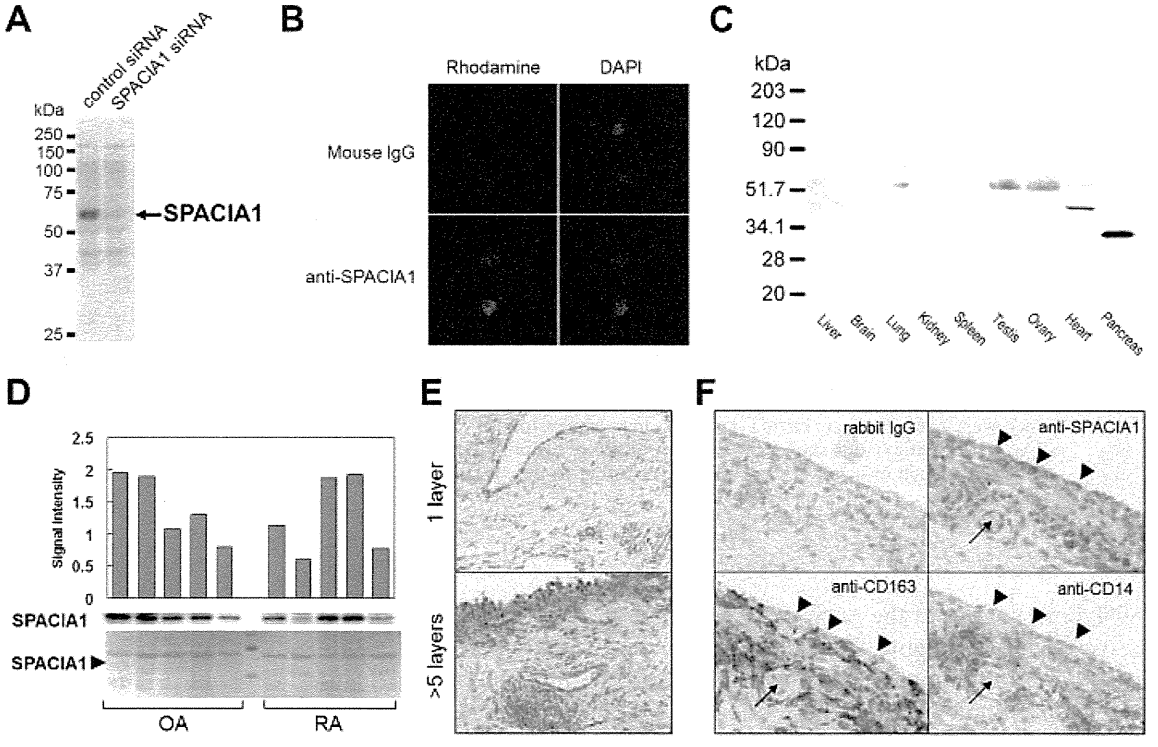

Figure 3. Expression analysis of SPACIA1 in human tissue. **A**, Western blotting of RASFs that were transfected with control or *SPACIA1* siRNA; an anti-SPACIA1 monoclonal antibody (mAb) was used for detection. **B**, Subcellular localization of SPACIA1 in RASFs. Immunofluorescence staining was performed with an anti-SPACIA1 mAb and normal mouse IgG. The images are representative of 3 separate experiments. **C**, Western blotting of various human tissues with an anti-SPACIA1 polyclonal antibody. **D**, Comparison of SPACIA1 expression levels in osteoarthritis (OA) and RA synovial tissue, by Western blotting. The membrane was stained with ponceau S to ensure equal protein loading in all lanes. The intensity of the SPACIA1-specific bands was quantified by densitometry. Another set of Western blots also showed no significant differences between RA and OA (data not shown). **E**, Expression of SPACIA1 in human synovium with or without hyperplasia of the synovial lining. SPACIA1-positive cells are brown. The images are representative of the results obtained in experiments with specimens from 5 different patients with RA or OA. Original magnification × 100. **F**, Localization of SPACIA1, CD163, and CD14 in serial sections of RA synovial membrane. **Arrowheads** show SPACIA1-positive, CD163-negative, and CD14-negative cells. **Arrows** show a capillary blood vessel. Original magnification × 200. See Figure 1 for other definitions.

genes (see Supplementary Table 1, available at http://onlinelibrary.wiley.com/journal/10.1002/(ISSN)1529-0131), we identified the top 15 genes ranked by their proliferative inhibition rate. Subsequently, by using siRNA against these genes (Supplementary Table 2 http://onlinelibrary.wiley.com/journal/10.1002/(ISSN)1529-0131), we reduced the number of genes associated with synoviocyte proliferation to 8 candidates (Figure 1). Among them, there were 2 genes with unknown functions. We named these genes synoviocyte proliferation–associated in collagen-induced arthritis 1 (*SPACIA1*) (GenBank accession no. AB489136 [human] and AB489137 [mouse]) and *SPACIA2* (GenBank accession no. AB541014 [human isoform 1], AB541015 [human isoform 2], and AB541013 [mouse]). The proliferation of RASFs was most strongly inhibited by *SPACIA1* siRNA, followed by lactotransferrin (*LTF*), proteinase 3 (*PRTN3*), glycine amidinotransferase (*GATM*), *SPACIA2*, placenta-specific gene 8 (*PLAC8*), peptidoglycan recognition protein 1 (*PGLYRP1*), and interleukin 6 (*IL6*). Therefore, we focused upon the role of *SPACIA1*.

Characterization of human and mouse *SPACIA1*. According to the NCBI nucleotide database (http://www.ncbi.nlm.nih.gov/nuccore), *SPACIA1* is identical to serum amyloid A–like 1 (*SAAL1*). The human and mouse *SPACIA1*/*SAAL1* genes are localized to chromosomes 11p15.1 and 7B4, respectively. These loci contain a gene cluster of the serum amyloid A (SAA) superfamily, which includes *SAA1*, *SAA2*, *SAA3*, and *SAA4* (16). The human and mouse SPACIA1/SAAL1 proteins are

Table 1. Correlation between expression level of SPACIA1 and pathologic features of synovitis in patients with RA or OA*

Feature	Low SPACIA1 expression, no. of patients	High SPACIA1 expression, no. of patients	P†
Synovial lining thickness			
Score 0–1 (≤4 layers)	9 (5 RA, 4 OA)	2 (0 RA, 2 OA)	
Score 2–3 (>4 layers)	0	7 (4 RA, 3 OA)	0.0011
Stromal cell density			
Score 0–1 (normal–mild)	8 (4 RA, 4 OA)	6 (1 RA, 5 OA)	
Score 2–3 (moderate–severe)	1 (1 RA, 0 OA)	3 (3 RA, 0 OA)	0.2882
Inflammatory cell infiltration			
Score 0–1 (normal–mild)	5 (2 RA, 3 OA)	2 (0 RA, 2 OA)	
Score 2–3 (moderate–severe)	4 (3 RA, 1 OA)	7 (4 RA, 3 OA)	0.1674

* Synovial tissue samples from 9 patients with rheumatoid arthritis (RA) and 9 patients with osteoarthritis (OA) were classified as having high or low expression of SPACIA1 based on the intensity of SPACIA1-specific bands shown on Western blotting. Synovial lining thickness, stromal cell density, and inflammatory cell infiltration were scored according to the synovitis grading system described by Krenn et al (1).
† Versus score of 0–1, by Fisher's exact test.

82% and 80% homologous at the nucleotide and amino acid levels, respectively (Figure 2). Furthermore, the NCBI HomoloGene database (http://www.ncbi.nlm.nih.gov/homologene) indicates that the sequence of the *SPACIA1/SAAL1* gene (unique identifier no. 34706) is conserved from zebrafish to humans. Although SPACIA/SAAL1 does not have any signal peptides, transmembrane domains, classic nuclear localization signals, or nuclear export signals, the InterPro database (http://www.ebi.ac.uk/interpro/) indicates that it has an armadillo-type motif (InterPro accession no. IPR016024) between amino acids 82 and 211 (Figure 2). In addition, previous proteomic studies showed that human and mouse SPACIA1/SAAL1 are phosphoproteins (Figure 2) .

The SAA protein family includes acute-phase proteins that are secreted in response to inflammation (19). Two members of this family, SAA1 and SAA2, are precursors of amyloid A, which causes amyloidosis secondary to RA (20). Thus, SAA plays an important role in inflammatory conditions, such as RA. However, the amino acid sequence of *SPACIA1* was not very similar to that of *SAA*; *SPACIA1* and *SAA1* are only 27% homologous. Moreover, unlike SAA proteins, which have a signal peptide and a conserved SAA domain, human and mouse SPACIA1/SAAL1 do not have either of these characteristics. As a result, we refer to SPACIA1/SAAL1 below as SPACIA1.

Expression analysis of human SPACIA1. Human SPACIA1 is a 55-kd protein that is expressed in RASFs (Figure 3A) and is predominantly localized to the nuclei (Figure 3B). In addition, SPACIA1 was strongly expressed in the testis and ovary, but only weakly expressed in the lung, spleen, and heart (Figure 3C). A 40-kd protein in the heart and a 30-kd protein in the pancreas were also detected with the anti-SPACIA1 pAb, but these results may have been due to nonspecific binding. Although SPACIA1 was also expressed abundantly in the synovial tissue of patients with RA or OA (Figure 3D), we did not observe any specific pattern in the expression levels of SPACIA1 in RA or OA synovial tissue. However, the expression level of SPACIA1 was significantly correlated with the thickness of the synovial lining, but not with the density of stromal cells or inflammatory cell infiltrates (Table 1). As expected from these results, SPACIA1 was strongly expressed in the hyperplastic synovial lining and moderately expressed in synovial stromal cells, endothelial cells, and plasma cells (Figure 3E). Interestingly, the localization of SPACIA1-positive cells was the opposite of that of CD14- or CD163-positive cells, which are considered to be synovial macrophages (Figure 3F).

Antiproliferative effect of *SPACIA1* siRNA in synovial fibroblasts. As shown in Figure 4A, *SPACIA1* siRNA inhibited the proliferation of RASFs that were stimulated with 10% FBS. However, this effect was significantly weaker than that of the positive control, c-*fos* siRNA, which strongly inhibits the proliferation of RASFs (21). On the other hand, the inhibitory effect of *SPACIA1* siRNA on the proliferation of RASFs that were stimulated with TNFα was comparable to that of *c-fos* siRNA (Figure 4B). Furthermore, flow cytometric analysis demonstrated that transfection of *SPACIA1* siRNA into RASFs increased the number of cells in the

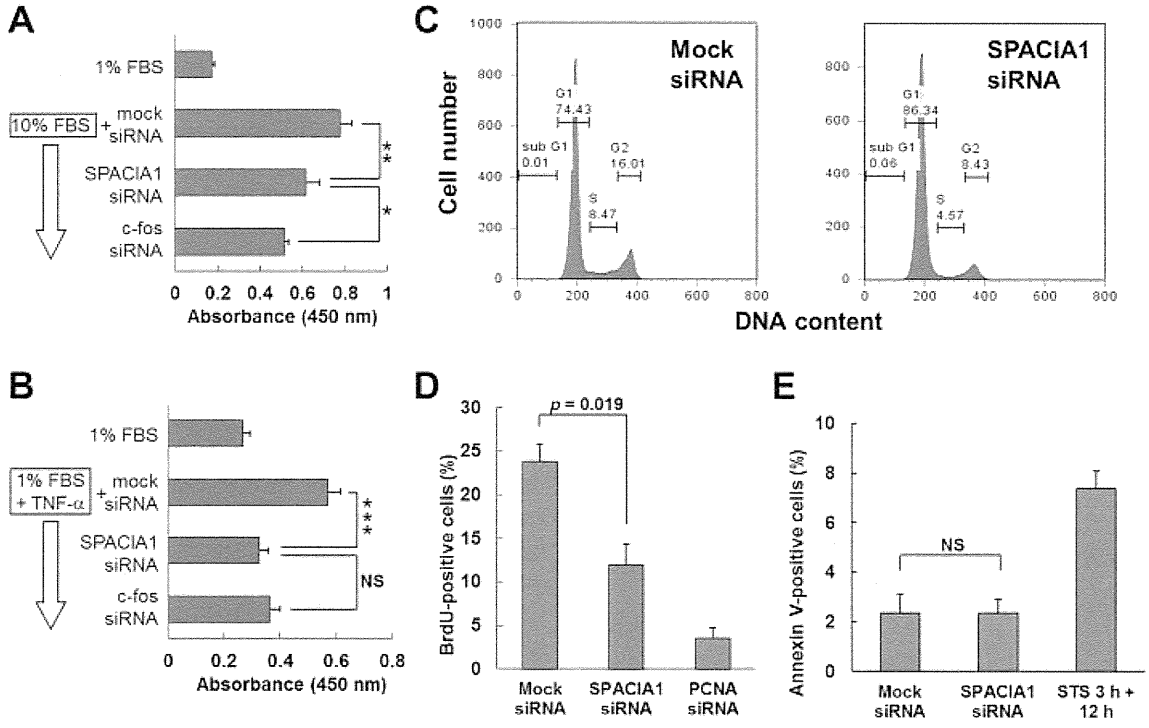

Figure 4. Antiproliferative effect of *SPACIA1* siRNA on RASFs by partial inhibition of entry into the S phase. **A** and **B**, *SPACIA1* siRNA suppressed the proliferation of RASFs in response to 10% fetal bovine serum (FBS) (**A**) or 5 ng/ml tumor necrosis factor α (TNFα) (**B**); c-*fos* siRNA was used as a positive control. Data are representative of 5 separate experiments in **A** and 3 separate experiments in **B**. Values are the mean ± SD. * = $P < 0.05$; ** = $P < 0.01$; *** = $P < 0.001$. NS = not significant. **C**, After culture of RASFs in medium supplemented with 10% FBS, *SPACIA1* siRNA reduced the number of RASFs in the S and G_2/M phase, compared with mock siRNA. Representative histograms from 3 different experiments are shown. **D**, After culture of RASFs in medium supplemented with 10% FBS, *SPACIA1* siRNA significantly inhibited the entry of RASFs into the S phase in a bromodeoxyuridine (BrdU) incorporation assay, compared with mock siRNA. *PCNA* siRNA was used as a positive control. Values are the mean ± SD (n = 3 experiments). **E**, After culture of RASFs in medium supplemented with 10% FBS, *SPACIA1* siRNA did not induce apoptosis in an annexin V apoptosis assay. RASFs that were treated with staurosporine (STS) for 3 hours and cultured for 12 hours were used as a positive control. Values are the mean ± SD. Experiments in **A, B, D,** and **E** were performed in triplicate. See Figure 1 for other definitions.

G_0/G_1 phase and reduced the number of cells in the S and G_2/M phase compared with mock siRNA transfection (Figure 4C). A BrdU incorporation assay showed that the percentage of BrdU-positive RASFs was 24%, 12%, and 4% after transfection with mock, *SPACIA1*, or *PCNA* siRNA, respectively (Figure 4D). Moreover, the percentage of annexin V–positive RASFs was similar after transfection with *SPACIA1* and mock siRNA (Figure 4E).

Progression of CIA in transgenic mice overexpressing *SPACIA1*. A schematic representation of the mammalian expression construct that was used to create transgenic mice overexpressing *SPACIA1* is shown in Figure 5A. The overexpression of *SPACIA1* in the transgenic mice was confirmed by Western blotting (Figure 5B) and PCR (results not shown). These transgenic mice did not spontaneously develop arthritis or cancer. Since findings of a preliminary experiment suggested that *SPACIA1*-transgenic mice are more sensitive to CIA than wild-type mice, we reduced the amount of CII that was used to induce arthritis, to more easily detect the difference in their sensitivity to CIA. Despite this modification, the incidence of CIA in the transgenic mice increased significantly more rapidly than in the wild-type mice, particularly at 30–37 days after the first injection of collagen (Figure 5C). Furthermore, the arthritis score in the paws of transgenic mice with CIA was significantly higher than that of wild-type mice at 30–39 days after the first injection (Figure 5D), and the histopathologic scores of the knee joints of the transgenic mice were significantly higher than in the wild-type mice (Figure 5E). Finally, immunohistochemistry was

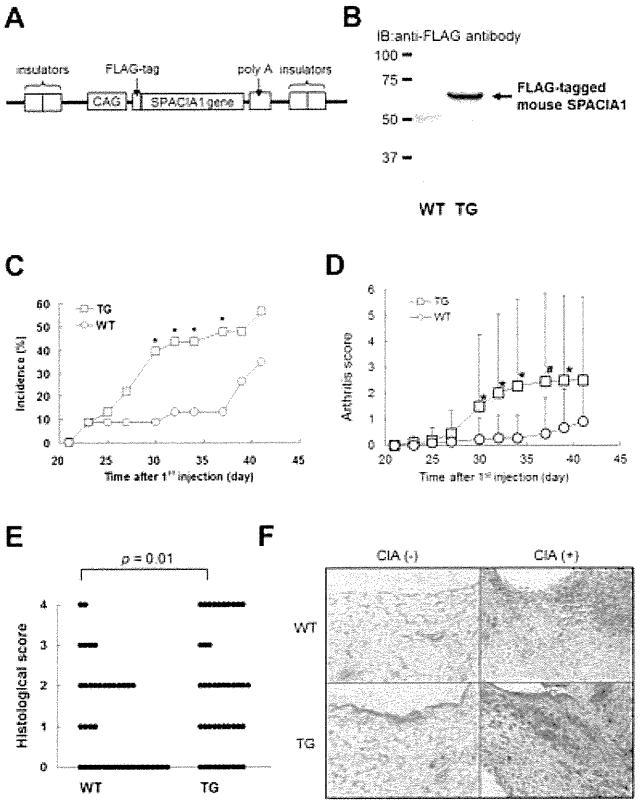

Figure 5. Early onset and rapid progression of collagen-induced arthritis (CIA) in transgenic (Tg) mice overexpressing *SPACIA1*. **A**, Schematic representation of the transgene for overexpression of mouse *SPACIA1*. **B**, Immunoblot (IB) analysis of lysates from tail tissue of wild-type (WT) and Tg mice, using an anti-FLAG antibody. **C**, Development of arthritis in 23 WT and 23 Tg mice after injection of bovine type II collagen (CII) on days 0 and 21. Arthritis incidence was significantly higher in Tg mice than in WT mice on days 30–37. $* = P < 0.05$ versus WT mice. **D**, Arthritis severity in 23 WT and 23 Tg mice after injection of CII on days 0 and 21. Arthritis scores were significantly higher in Tg mice than in WT mice on days 30–39. Values are the mean ± SD. $* = P < 0.05$; $\# = P < 0.01$, versus WT mice. **E**, Histopathologic scores in the knee joints of 23 WT and 23 Tg mice after injection of CII on days 0 and 21. **F**, Expression of SPACIA1 protein in synovial tissue from the knee joints of WT and Tg mice with or without CIA. Original magnification × 100.

performed to examine the expression levels of SPACIA1 protein in the joints of the mice with CIA (Figure 5F). The number of SPACIA1-positive cells was markedly increased in the joints of both wild-type and transgenic mice with CIA.

DISCUSSION

In this study of ~36,000 mRNA transcripts, we identified a novel gene, *SPACIA1*, that is involved in the dysregulated proliferation of synovial fibroblasts in the foot joints of mice with CIA. However, since the forepaw tissue samples included not only synovium but also bone, cartilage, muscle, and tendon tissue, the transcriptome analysis was not specific for genes that are expressed in the synovium. To overcome this problem, we used human RASFs to screen the candidate genes that were identified from the transcriptome analysis. We found that SPACIA1 was expressed not only in cultured RASFs (Figure 3A and B) but also in the inflamed joints of mice and humans (Figures 3E and 5F). Notably, SPACIA1 was strongly expressed in synovial fibroblasts, and not in synovial macrophages, in the intimal layer of the synovial membrane of human RA patients (Figure 3F). Furthermore, its expression in human synovial tissue was not specific to RA, as was demonstrated by its expression in synovial tissue from patients with OA as well (Figure 3D). Similar to RA, synovitis commonly occurs in end-stage OA (22). In fact, 90% of joints from OA patients undergoing arthroplasty contain pannus-like tissue on the articular surface (23). As a result, SPACIA1 may be expressed at comparable levels in OA and RA synovia.

Transgenic mice overexpressing *SPACIA1* exhibited earlier onset and more rapid progression of CIA than wild-type mice (Figures 5C–E). In addition, the expression level of SPACIA1 was positively correlated with the thickness of the synovial lining in humans (Table 1). These results suggest that overexpression of SPACIA1 accelerates the progression of synovitis by promoting synovial cell proliferation. However, it is unlikely that SPACIA1 overexpression affected the immune system, because we did not observe any significant difference in the ratio of spleen weight to body weight between the wild-type and transgenic mice with CIA (data not shown). In addition, there were no significant differences in anti-CII antibody titers in serum from the wild-type and transgenic mice with CIA (data not shown). With regard to the use of transgenic mice overexpressing FLAG-tagged mouse SPACIA1, there is both a benefit and a limitation that should be considered. The benefit is that FLAG-tagged mouse SPACIA1 is easy to distinguish from endogenous mouse SPACIA1. The limitation is that we were not able to identify any potential side effects of the FLAG tag when we evaluated these transgenic mice. However, to minimize this potential effect, we confirmed that there are no significant domains in the N-terminal region of SPACIA1, e.g., a signal peptide.

Since *SPACIA1* knockdown inhibited synoviocyte proliferation, our results indicate that SPACIA1 should

be implicated in the abnormal proliferation of synovial fibroblasts in synovitis due to an antiapoptotic effect or stimulation of cell cycle progression. In this regard, although *SPACIA1* knockdown inhibited the entry of RASFs into the S phase (Figures 4C and D), it did not induce apoptosis in RASFs (Figure 4E). In addition, our ongoing studies indicate that *SPACIA1* knockdown halves the expression of the genes for cyclin E2 and cyclin-dependent kinase 2, which are involved in the progression of the cell cycle from G_1 to S (Sato T, et al: unpublished observations). Therefore, it is more likely that SPACIA1 regulates the progression of the cell cycle than that it regulates apoptosis in RASFs.

What is the possible mechanism of action of SPACIA1? When we screened the molecules that interact with SPACIA1 using a yeast 2-hybrid assay, most of the molecules obtained were transcription regulatory factors that are located in the nucleus (data not shown). This suggests that SPACIA1 might act as a transcriptional regulator by forming a complex with certain molecules in the nucleus. We next considered the setting in which SPACIA1 acts. Because serum contains a variety of growth factors and hormones, the addition of serum to the culture medium represents a general stimulation that leads to proliferation of cells, whereas administration of TNFα represents an inflammatory stimulation that induces cell proliferation. Since *SPACIA1* knockdown was more efficient at blocking TNFα-induced proliferation than serum-induced proliferation (Figures 4A and B), SPACIA1 might be especially involved in the inflammatory signaling pathways that induce the proliferation of RASFs. Based on our findings, we speculate that SPACIA1 may act downstream of inflammatory signaling and regulate the transcription of cell cycle–implicated genes, which then regulate the expression of cyclin E2 and cyclin-dependent kinase 2. However, further investigation is needed to clarify the precise mechanism of action of SPACIA1, e.g., whether it affects any of the major signaling pathways, including the NF-κB or JNK pathway.

Moreover, there is in vivo evidence that the effect of SPACIA1 on synoviocyte proliferation is limited to inflammatory conditions. The transgenic mice overexpressing *SPACIA1* did not spontaneously develop arthritis or cancer, and administration of a collagen emulsion was still required for induction of synoviocyte proliferation. Therefore, unlike typical anticancer drugs, an SPACIA1 inhibitor may be able to specifically suppress abnormal synoviocyte proliferation in inflammatory environments with relatively few side effects.

In conclusion, the overexpression of SPACIA1, a novel protein that is involved in the proliferation of synovial fibroblasts, is associated with the progression of synovitis in mice and humans. Consequently, SPACIA1 might be a potential therapeutic target for inhibiting synovial proliferation in RA and OA.

ACKNOWLEDGMENTS

We would like to thank N. Watanabe-Asakura, K. Takahashi, N. Yamamoto, A. Une, N. Furuya, S. Shinkawa, Y. Nakagawa, K. Suzuki, S. Asada, T. Sato-Mogi, H. Ogasawara, Y. Sato, Y. Urbanczyk, M. Yamanashi, and M. Ishikawa for excellent technical assistance.

AUTHOR CONTRIBUTIONS

All authors were involved in drafting the article or revising it critically for important intellectual content, and all authors approved the final version to be published. Dr. Fujii had full access to all of the data in the study and takes responsibility for the integrity of the data and the accuracy of the data analysis.

Study conception and design. Fujii, Konomi, Nishioka, Nakajima.
Acquisition of data. Sato, Fujii, Konomi, Yagishita, Aratani, Araya.
Analysis and interpretation of data. Sato, Fujii, Konomi, Yagishita, Aratani, Araya, Aono, Yudoh, Suzuki, Beppu, Yamano, Nishioka, Nakajima.

ROLE OF THE STUDY SPONSOR

Santen Pharmaceutical collaborated with St. Marianna University School of Medicine in this study. Employees of Santen Pharmaceutical contributed to the study design, data collection, data analysis, and writing of the manuscript; however, Santen Pharmaceutical was not involved in the decision to submit the manuscript for publication or in approval of the content of the submitted manuscript, and publication of the manuscript was not contingent upon the approval of Santen Pharmaceutical.

REFERENCES

1. Krenn V, Morawietz L, Burmester GR, Kinne RW, Mueller-Ladner U, Muller B, et al. Synovitis score: discrimination between chronic low-grade and high-grade synovitis. Histopathology 2006; 49:358–64.
2. Ritchlin C. Fibroblast biology: effector signals released by the synovial fibroblast in arthritis. Arthritis Res 2000;2:356–60.
3. Mueller-Ladner U, Gay R, Gay S. Structure and function of synoviocytes. In: Koopman W, editor. Arthritis and allied conditions: a textbook of rheumatology. 14th ed. Philadelphia: Lippincott Williams & Wilkins; 2001. p. 285–300.
4. Taniguchi K, Kohsaka H, Inoue N, Terada Y, Ito H, Hirokawa K, et al. Induction of the p16INK4a senescence gene as a new therapeutic strategy for the treatment of rheumatoid arthritis. Nat Med 1999;5:760–7.
5. Nasu K, Kohsaka H, Nonomura Y, Terada Y, Ito H, Hirokawa K, et al. Adenoviral transfer of cyclin-dependent kinase inhibitor genes suppresses collagen-induced arthritis in mice. J Immunol 2000;165:7246–52.
6. Appelboom T, Mann H, Senolt L, Suchy D, Nemec P, Rolova J, et al. Preliminary results of a phase I clinical trial of intra-articular administration of ARG098, a novel anti-Fas IgM mAb, in RA [abstract]. Arthritis Rheum 2009;60 Suppl:S156.

7. Amano T, Yamasaki S, Yagishita N, Tsuchimochi K, Shin H, Kawahara K, et al. Synoviolin/Hrd1, an E3 ubiquitin ligase, as a novel pathogenic factor for arthropathy. Genes Dev 2003;17: 2436–49.
8. Hughes C, Wolos JA, Giannini EH, Hirsch R. Induction of T helper cell hyporesponsiveness in an experimental model of autoimmunity by using nonmitogenic anti-CD3 monoclonal antibody. J Immunol 1994;153:3319–25.
9. Izumi T, Fujii R, Izumi T, Nakazawa M, Yagishita N, Tsuchimochi K, et al. Activation of synoviolin promoter in rheumatoid synovial cells by a novel transcription complex of interleukin enhancer binding factor 3 and GA binding protein α. Arthritis Rheum 2009;60:63–72.
10. Cooper H, Paterson Y. Preparation of polyclonal antisera. In: Ausubel F, Brent R, Kingston R, Moore D, Seldman J, Smith J, et al, editors. Current protocols in molecular biology. New York: John Wiley & Sons; 1997. p. 11.12.1–11.13.4.
11. Fuller S, Takahashi M, Hurrell J. Preparation of monoclonal antibodies. In: Ausubel F, Brent R, Kingston R, Moore D, Seldman J, Smith J, et al, editors. Current protocols in molecular biology. New York: John Wiley & Sons; 1997. p. 11.4.1–11.11.5.
12. Jiang W, Jimenez G, Wells NJ, Hope TJ, Wahl GM, Hunter T, et al. PRC1: a human mitotic spindle-associated CDK substrate protein required for cytokinesis. Mol Cell 1998;2:877–85.
13. Chung JH, Whiteley M, Felsenfeld G. A 5' element of the chicken β-globin domain serves as an insulator in human erythroid cells and protects against position effect in Drosophila. Cell 1993;74: 505–14.
14. Miyake-Nishijima R, Iwata S, Saijo S, Kobayashi H, Kobayashi S, Souta-Kuribara A, et al. Role of Crk-associated substrate lymphocyte type in the pathophysiology of rheumatoid arthritis in tax transgenic mice and in humans. Arthritis Rheum 2003;48: 1890–900.
15. Brackertz D, Mitchell GF, Mackay IR. Antigen-induced arthritis in mice. I. Induction of arthritis in various strains of mice. Arthritis Rheum 1977;20:841–50.
16. Sellar GC, Jordan SA, Bickmore WA, Fantes JA, van Heyningen V, Whitehead AS. The human serum amyloid A protein (SAA) superfamily gene cluster: mapping to chromosome 11p15.1 by physical and genetic linkage analysis. Genomics 1994;19:221–7.
17. Matsuoka S, Ballif BA, Smogorzewska A, McDonald ER III, Hurov KE, Luo J, et al. ATM and ATR substrate analysis reveals extensive protein networks responsive to DNA damage. Science 2007;316:1160–6.
18. Ballif BA, Villen J, Beausoleil SA, Schwartz D, Gygi SP. Phosphoproteomic analysis of the developing mouse brain. Mol Cell Proteomics 2004;3:1093–101.
19. Coetzee GA, Strachan AF, van der Westhuyzen DR, Hoppe HC, Jeenah MS, de Beer FC. Serum amyloid A-containing human high density lipoprotein 3: density, size, and apolipoprotein composition. J Biol Chem 1986;261:9644–51.
20. Baba S, Takahashi T, Kasama T, Shirasawa H. Identification of two novel amyloid A protein subsets coexisting in an individual patient of AA-amyloidosis. Biochim Biophys Acta 1992;1180: 195–200.
21. Morita Y, Kashihara N, Yamamura M, Okamoto H, Harada S, Kawashima M, et al. Antisense oligonucleotides targeting c-fos mRNA inhibit rheumatoid synovial fibroblast proliferation. Ann Rheum Dis 1998;57:122–4.
22. Samuels J, Krasnokutsky S, Abramson SB. Osteoarthritis: a tale of three tissues. Bull NYU Hosp Jt Dis 2008;66:244–50.
23. Shibakawa A, Aoki H, Masuko-Hongo K, Kato T, Tanaka M, Nishioka K, et al. Presence of pannus-like tissue on osteoarthritic cartilage and its histological character. Osteoarthritis Cartilage 2003;11:133–40.

RETROVIROLOGY

RESEARCH Open Access

Functional impairment of Tax-specific but not cytomegalovirus-specific CD8$^+$ T lymphocytes in a minor population of asymptomatic human T-cell leukemia virus type 1-carriers

Ayako Takamori[1], Atsuhiko Hasegawa[1*], Atae Utsunomiya[2], Yasuhiro Maeda[3,9], Yoshihisa Yamano[4], Masato Masuda[5], Yukiko Shimizu[4], Yotaro Tamai[1], Amane Sasada[1], Na Zeng[1], Ilseung Choi[6], Naokuni Uike[6], Jun Okamura[7], Toshiki Watanabe[8], Takao Masuda[1] and Mari Kannagi[1]

Abstract

Background: Human T-cell leukemia virus type 1 (HTLV-1) causes adult T-cell leukemia (ATL) and HTLV-1-associated myelopathy/tropical spastic paraparesis (HAM/TSP) in a small percentage of infected individuals. ATL is often associated with general immune suppression and an impaired HTLV-1-specific T-cell response, an important host defense system. We previously found that a small fraction of asymptomatic HTLV-1-carriers (AC) already showed impaired T-cell responses against the major target antigen, Tax. However, it is unclear whether the impaired HTLV-1 Tax-specific T-cell response in these individuals is an HTLV-1-specific phenomenon, or merely reflects general immune suppression. In this study, in order to characterize the impaired HTLV-1-specific T-cell response, we investigated the function of Tax-specific CD8$^+$ T-cells in various clinical status of HTLV-1 infection.

Results: By using tetramers consisting of HLA-A*0201, -A*2402, or -A*1101, and corresponding Tax epitope peptides, we detected Tax-specific CD8$^+$ T-cells in the peripheral blood from 87.0% of ACs (n = 20/23) and 100% of HAM/TSP patients (n = 18/18) tested. We also detected Tax-specific CD8$^+$ T-cells in 38.1% of chronic type ATL (cATL) patients (n = 8/21), although its frequencies in peripheral blood CD8$^+$ T cells were significantly lower than those of ACs or HAM/TSP patients. Tax-specific CD8$^+$ T-cells detected in HAM/TSP patients proliferated well in culture and produced IFN-γ when stimulated with Tax peptides. However, such functions were severely impaired in the Tax-specific CD8$^+$ T-cells detected in cATL patients. In ACs, the responses of Tax-specific CD8$^+$ T-cells were retained in most cases. However, we found one AC sample whose Tax-specific CD8$^+$ T-cells hardly produced IFN-γ, and failed to proliferate and express activation (CD69) and degranulation (CD107a) markers in response to Tax peptide. Importantly, the same AC sample contained cytomegalovirus (CMV) pp65-specific CD8$^+$ T-cells that possessed functions upon CMV pp65 peptide stimulation. We further examined additional samples of two smoldering type ATL patients and found that they also showed dysfunctions of Tax-specific but not CMV-specific CD8$^+$ T-cells.

Conclusions: These findings indicated that Tax-specific CD8$^+$ T-cells were scarce and dysfunctional not only in ATL patients but also in a limited AC population, and that the dysfunction was selective for HTLV-1-specifc CD8$^+$ T-cells in early stages.

* Correspondence: hase.impt@tmd.ac.jp
[1]Department of Immunotherapeutics, Tokyo Medical and Dental University, Tokyo, Japan
Full list of author information is available at the end of the article

Background

Human T-cells leukemia virus type 1 (HTLV-1) is the causative agent of a highly aggressive $CD4^+$ T-cell malignancy, adult T-cell leukemia (ATL)[1,2]. As many as 10 million individuals are thought to be infected worldwide, in southern Japan, the Caribbean basin, South America, Melanesia, and equatorial Africa[3]. Unlike human immunodeficiency virus (HIV), the majority of HTLV-1-infected individuals are clinically asymptomatic during their lifetime. However, approximately 5% develop ATL, and another 2-3% develop a variety of chronic inflammatory diseases such as HTLV-1-associated myelopathy/tropical spastic paraparesis (HAM/TSP)[4-8].

HTLV-1-specific cytotoxic T-lymphocytes (CTLs) are thought to play a pivotal role in containing the proliferation of HTLV-1-infected T-cells[9,10]. Tax is known to be the dominant target antigen for HTLV-1-specific CTLs[10-13], and a high frequency of Tax-specific CTLs can be detected in HAM/TSP patients and some asymptomatic HTLV-1 carriers (ACs)[10-14]. However, ATL patients show general immune suppression[15], reduced frequency and dysfunction of Tax-specific CTLs[16,17]. Regulatory T cell (Treg)-like function of $FoxP3^+$ ATL cells and diminished function of dendritic cells may be involved in the immune suppression in ATL patients [18,19], but the precise mechanism is not yet clarified. We previously demonstrated that a fraction of ACs also exhibit reduced T-cell responses against Tax protein [20]. These observations suggest that the reduced HTLV-1-specific T-cell response might be an underlying risk of ATL development, but not the result of ATL. However, it is unknown how the function of HTLV-1-specific $CD8^+$ T-cells becomes impaired in a small percentage of ACs and whether its dysfunction is specific for HTLV-1 antigen or due to general immune suppression.

During chronic stage of infection with several viruses, such as HIV and hepatitis C virus (HCV), virus-specific CTLs gradually lose their cytotoxic activity, the ability to proliferate and secrete a diverse profile of cytokines, ultimately leading to exhaustion, anergy or even deletion of these cells[21-26]. Programmed death-1 (PD-1), a negative regulator in the CD28 superfamily, has recently been shown to be highly expressed on virus-specific T-cells during many chronic viral infections[27-29]. It has also been reported that the interaction of PD-1 with PD-ligand 1 (PD-L1) negatively regulates cytokine production and proliferation of T-cells[30,31]. A previous report indicates that PD-1 is up-regulated on the dominant Tax-specific CTLs in ATL patients and ACs and that immune regulation through the PD-1/PD-L1 pathway may be involved in the dysfunction of HTLV-1-specific CTLs in ATL patients[32].

Studies on memory T-cell differentiation have shown that phenotype, function, and homeostasis of memory T-cells vary for different persistent virus infections[33]. Central memory T-cells (T_{CM}; $CD45RA^-CCR7^+$) are elicited by non-persisting virus that provide transient antigen stimulation, such as in Influenza virus infection. In contrast, effector memory T-cells (T_{EM}; $CD45RA^-CCR7^-$) predominate when relatively high levels of antigen persist, such as in HIV infection. Terminally differentiated memory (T_{Diff}; $CD45RA^+CCR7^-$) can be seen when antigen persists at a low level, such as in cytomegalovirus (CMV) infection. In HTLV-1 infection, it has been reported that dominant Tax-specific CTLs in HAM/TSP patients consist of T_{EM} and T_{Diff} compartments[34].

We previously identified some major epitopes recognized by HTLV-1-specific CTLs in infected individuals carrying HLA-A2, -A11, or -A24[12,35,36]. These allowed us to monitor HTLV-1-specific CTLs and analyze their functions *ex vivo*, by using antigen/HLA tetrameric complexes. In this study, we demonstrate that IFN-γ production and proliferative capacity of tetramer-binding Tax-specific $CD8^+$ T-cells were severely impaired not only in ATL patients but also in a minor population of asymptomatic HTLV-1 carriers (ACs). Importantly, the T-cell dysfunction at the asymptomatic stage was selective for HTLV-1 but not for CMV antigen. In addition, severely impaired HTLV-1-specific but not CMV-specific $CD8^+$ T-cells responses were also observed in patients diagnosed as smoldering ATL, the clinical condition of which is close to that of AC. The dysfunction of HTLV-1-specific $CD8^+$ T-cells in an early clinical stage implies HTLV-1-specific immune suppressive mechanism might be an underlying risk for ATL.

Results

Incidence and frequency of Tax-specific $CD8^+$ T-cells in ACs, and HAM/TSP and cATL patients

In 23 ACs and 18 HAM/TSP and 21 cATL patients carrying HLA-A2, -A11 and/or -A24 alleles, we evaluated the frequencies of Tax-specific $CD8^+$ T-cells by using cognate Tax/HLA tetramers (Figure 1 and Table 1). Tax-specific $CD8^+$ T-cells were detected in 87.0% of ACs and all HAM/TSP patients tested. In contrast, only 38.1% of cATL patients have detectable frequencies of Tax-specific $CD8^+$ T-cells (Table 1). Figure 1B shows that the average frequency of Tax-specific $CD8^+$ T-cells in the $CD8^+$ T-cells of cATL patients (n = 21, 0.90% range: 0%-9.45%) was significantly lower than that in ACs (n = 23, 2.37%, range: 0%-8.23%, $P = 0.0023$). HAM/TSP patients had the highest average frequency of Tax-specific $CD8^+$ T-cells among the three groups (n = 18, 8.88%, range: 1.86%-29.9%, $P = 0.0001$; vs. AC, $P < 0.0001$; vs. cATL patients), which is consistent with

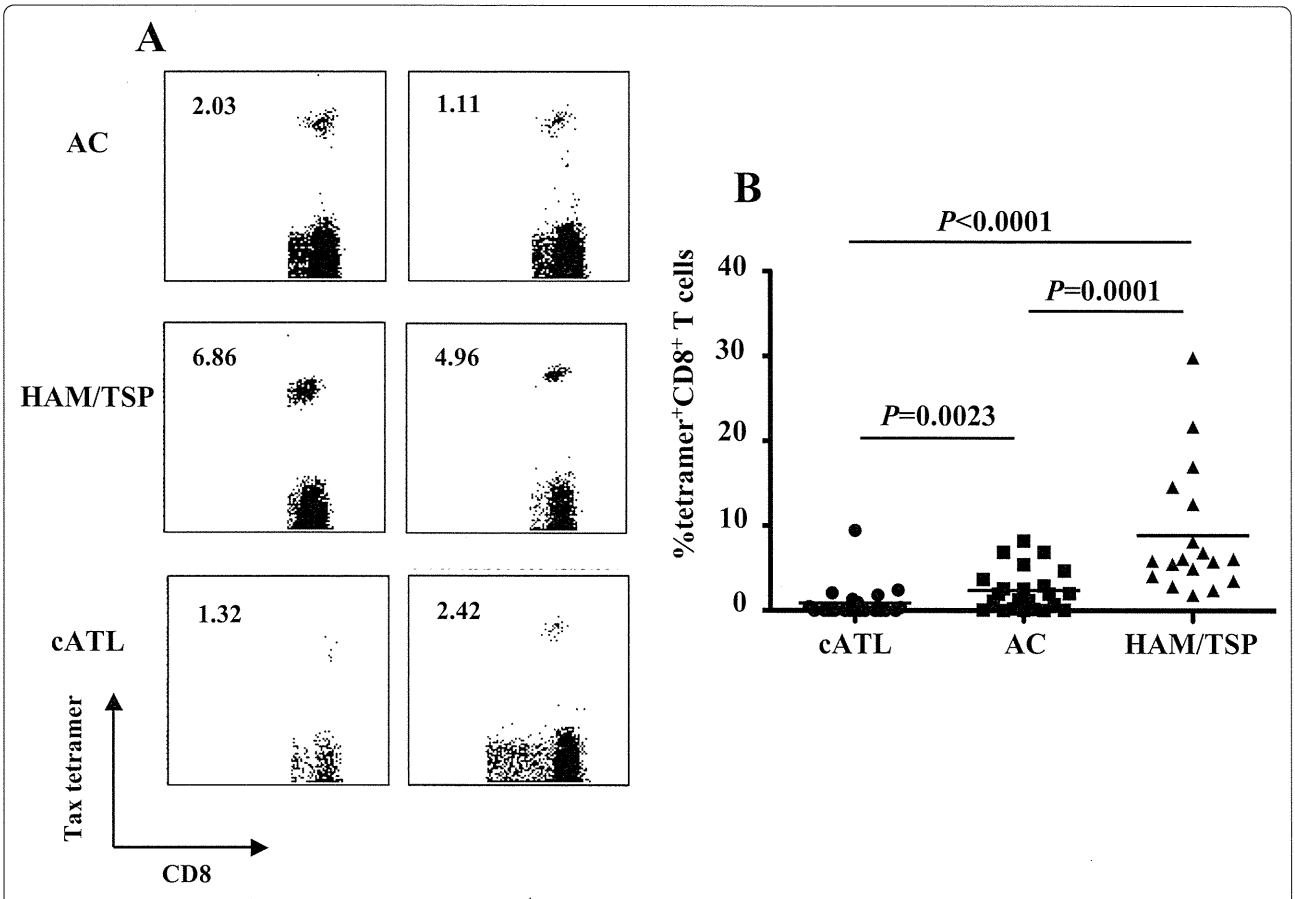

Figure 1 Incidence and frequency of Tax-specific CD8$^+$ T-cells in ACs, and HAM/TSP and cATL patients. (A) Whole blood or PBMCs from AC (top), and HAM/TSP (middle) and cATL (bottom) patients were stained with Tax/HLA tetramer. Number indicates the percentage of tetramer$^+$ cells in CD8$^+$ T-cells. (B) The percentage of Tax-tetramer$^+$ CD8$^+$ T-cells in AC (n = 23), and HAM/TSP (n = 18) and cATL (n = 21) patients. *P* value was determined by the Mann-Whitney *U* test. Horizontal bars indicate the average percentage of Tax-tetramer$^+$ CD8$^+$ T-cells for the group.

previous reports [10,17,37]. It is of note that Tax-specific CD8$^+$ T-cells are detectable even in cATL patients, although the frequency is very low.

Impaired cell proliferation and IFN-γ production of Tax-specific CD8$^+$ T-cells in cATL but not HAM/TSP patients

We next examined IFN-γ production and cell proliferation of Tax-specific CD8$^+$ T-cells in HAM/TSP and cATL patients (Figure 2A). Intracellular IFN-γ staining showed that Tax-specific CD8$^+$ T-cells in all HAM/TSP patients tested produced IFN-γ when stimulated with Tax peptide (Figure 2A). Tax-specific CD8$^+$ T-cells in those HAM/TSP patients proliferated regardless of stimulation with Tax peptide (Figure 2B). In contrast to HAM/TSP patients, IFN-γ production from Tax-specific CD8$^+$ T-cells in a cATL patient was hardly detectable even when stimulated with Tax peptide (4.8%, Figure 2A). In the same donor, Tax-specific CD8$^+$ T-cells

Table 1 The number of blood samples with detectable Tax-specific CD8$^+$ T-cells in all samples tested in this study

Tax/HLA tetramers used in this study	Disease Status		
	AC	HAM/TSP	cATL
HLA-A*0201/Tax11-19	12/14[1]	7/7	2/11
HLA-A*1101/Tax88-96	4/4	4/4	3/5
HLA-A*2402/Tax301-309	13/15	13/13	5/16
No. of tetramer$^+$ samples/total no. of blood samples[2]	20/23 (87.0%)	18/18 (100%)	8/21 (38.1%)

[1] No. of samples with detectable Tax-specific CD8$^+$ T-cells/total no. of samples carrying each HLA allele. When the frequency of tetramer$^+$ cells was more than 0.04% of CD8$^+$ T-cells, the sample was regarded as detectable.

[2] In case Tax-specific CD8$^+$ T-cells was detectable by either tetramer in a sample carrying two of three HLA-A alleles above, the sample was regarded as positive.

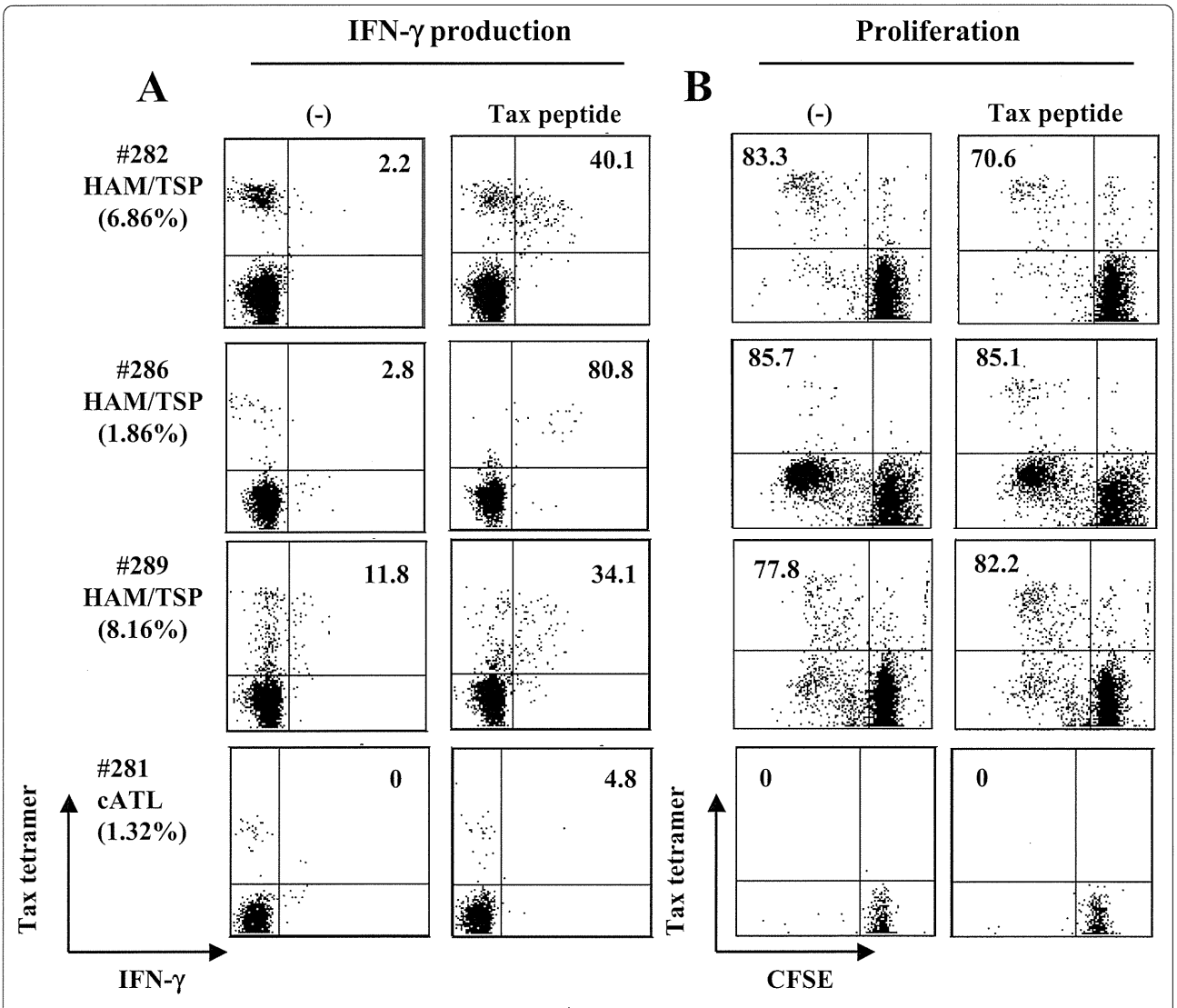

Figure 2 IFN-γ production and proliferation of Tax-specific CD8$^+$ T-cells in HAM/TSP and cATL patients. (A) PBMCs from HAM/TSP and cATL patients were stimulated with or without 10 μM Tax peptide for 6 hrs. The number indicates the percentage of IFN-γ-producing cells in tetramer$^+$ cells. (B) For CFSE-based T-cell proliferation, CFSE-labeled PBMCs from HAM/TSP and cATL patients were cultured in the presence or absence of 100 nM Tax peptide for 6 days. The number indicates the percentage of dividing (CFSE^{low}) cells in tetramer$^+$ cells. The percentage of tetramer$^+$ cells among CD8$^+$ T cells in fresh blood is indicated in parenthesis under the patient ID.

could be detected in fresh blood (1.32%) and after 6 hrs incubation as shown in Figure 2A, but not after 6 day-culture, suggesting that Tax-specific CD8$^+$ T-cells in this cATL patient had no proliferative capacity (Figure 2B). We tested PBMC from four other cATL patients who had detectable Tax-specific CD8$^+$ T-cells, but none of them showed proliferation of Tax-specific CD8$^+$ T-cells by either the CFSE-based proliferation assay or 13-day culture (Additional file 1). Collectively, these results indicate that Tax-specific CD8$^+$ T-cells from most cATL patients are impaired in their capacities to proliferate and produce IFN-γ.

Diversity in the IFN-γ production and cell proliferation of Tax-specific CD8$^+$ T-cells in ACs

Our recent studies using the GST-Tax protein-based assay demonstrated that the extent of Tax-specific T-cell responses varied widely in ACs[20]. We then evaluated proliferation and/or IFN-γ production of tetramer-binding Tax-specific CD8$^+$ T-cells in 14 ACs (Table 2). Representative data on 4 of 14 ACs are shown in Figures 3A and 3B. In 3 ACs (#251, #313, and #360), Tax-specific CD8$^+$ T-cells produced IFN-γ and proliferated in response to Tax peptide (Figures 3A and 3B). Similarly to HAM/TSP samples, a large proportion of Tax-

Table 2 Clinical information and summary for Tax-specific CD8$^+$ T cells in 14ACs

ID	Age	Sex	WBC (/μl)	CD4 (%)[1]	CD8 (%)[1]	HLA	Tetramer (%)[2]	Functions and phenotype of Tax-specific CD8$^+$ T-cells[3]			Ably (%)[7]	PVL[8]
								IFN-γ$^+$ (%)[4]	CFSE^{low} (%)[5]	PD-1$^+$ (%)[6]		
#217	70s	F	6800	ND[9]	5.72	A24	1.94	27.7	78.9	78.7	0	14
#236	30 s	F	6500	ND	11.9	A24	2.54	31.1	0	54.1	0	22
#238	60 s	F	5700	ND	12.7	A11	1.29	36.4	100	0	0	2
#243	50 s	F	4100	ND	24.6	A2/24	0.39/3.67	11.3	27.6	93.8	0	3
#245	40 s	F	5000	ND	22.6	A2	0.73	62.5	75	ND	1	58
#251	60 s	M	4800	ND	11.9	A2/11	0.70/8.23	35.8	84.4	36.7	0	2
#279	40 s	M	6200	34.1	11.6	A2/24	4.70/0.18	12.9	30.8	70.2	1	48
#287	70 s	M	4800	72.5	10.0	A2/24	1.17/0.23	11.1	0	55.6	2	81
#309	60 s	F	4600	37.5	24.8	A11/24	6.88/4.26	51.7	76.2	85.3	1.5	29
#311	60 s	F	3200	30.6	14.8	A2/24	1.02/1.94	51.3	ND	ND	0	6
#312	50 s	F	2700	27.3	36.4	A24	2.03	77.8	ND	ND	ND	UN[10]
#313	60 s	M	7300	25.4	31.0	A24	1.11	55.7	60	90.6	ND	4
#315	50 s	F	7500	26.5	7.9	A2/24	6.88/0	24.5	84.7	20	0.6	17
#360	50 s	M	6200	37.7	29.9	A2	2.6	63.1	68.4	10.2	0	UN

[1]The number indicates percentage of CD4$^+$ or CD8$^+$ T cells in lymphocytes.

[2]The number indicates percentages of tetramer$^+$ cells in CD8$^+$ T-cells. Two numbers divided by a slash represent those detected by two different tetramers corresponding to two HLA alleles shown in the HLA column.

[3]In case of a sample carrying two of three HLA-A alleles (A2, A11, or A24), Tax-specific CTLs predominantly detected by a tetramer were used. The number represents percentage of indicated cells in the tetramer-binding CD8$^+$ T cells.

[4]Evaluated by intracellular IFN-γ staining following 6 hours stimulation with corresponding Tax peptide.

[5]Evaluated by CFSE intensities in labeled PBMC after 6 days incubation with corresponding Tax peptide stimulation.

[6]The number represents percentage of indicated PD-1$^+$Tax-specific CD8$^+$ T cells without culture.

[7]Ably; abnormal lymphocytes

[8]PVL; proviral load. The number represents copy number per 1000 PBMCs.

[9]ND; not determined

[10]UN; undetectable

specific CD8$^+$ T-cells in these ACs spontaneously proliferated without stimulation with Tax peptide, probably due to viral reactivation in HTLV-1-infected cells *in vitro*[38,39]. IFN-γ production was specifically detected for peptide stimulation, and 35.8-55.7% of Tax-specific CD8$^+$ T-cells produced a good amount of IFN-γ (mean fluorescence intensity, MFI: 63.7-195.3) upon stimulation in the samples of #251, #313, and #360. In contrast, Tax-specific CD8$^+$ T-cells in one AC (#287) did not proliferate in response to Tax peptide and showed a very weak IFN-γ response with low amounts of IFN-γ (MFI: 37.5) in a low percentage (11.1%) of Tax-specific CD8$^+$ T-cells (Figures 3A and 3B). In other ACs (#243 and #279), low frequency of IFN-γ$^+$ Tax-specific CD8$^+$ T-cells was observed, but the levels of IFN-γ production (MFI: #243; 58.8, #279; 77.6) and the proliferative responses were comparable to other ACs (Table 2). Tax-specific CD8$^+$ T-cells in #236 failed to proliferate but showed favorable IFN-γ production (MFI: 80.1) in 31.1% of the cells.

Among AC samples tested, AC#287 carried higher proviral load (81 copies in 1000 PBMCs) than any other ACs (Table 2). Since Tax-specific CD8$^+$ T-cells in #287 had severely impaired IFN-γ production and proliferative potential, we examined the relationship of the function of these T-cells with proviral loads. Both percentages of IFN-γ$^+$ and dividing Tax-specific CD8$^+$ T-cells among CD8$^+$ T-cells were likely to be inversely correlated with proviral loads although they were not statistically significant (Figure 3C and 3D). Because of the limited availability of the samples, we focused mainly on two ACs (#287 and #313) in the studies hereafter.

Dysfunction of Tax-specific CD8$^+$ T-cells and inefficient CD8$^+$ cell-mediated HTLV-1 control in AC #287

To examine whether Tax-specific CD8$^+$ T-cell responses were influenced by activation of antigen-presenting cells (APCs), PBMC from #313 (responder) and #287 (low responder) were stimulated with Tax peptide in the presence or absence of LPS, a potent activator of APCs such as dendritic cells (DCs) and monocytes/macrophages. In #313, the frequency of Tax-specific CD8$^+$ T-cells increased from 1.11% to 6.47% or 4.07% at day 13, after stimulation with or without Tax peptide, respectively. The frequency of Tax-specific CD8$^+$ T-cells in #313 further increased in the presence of Tax peptide and LPS (15.81%). In contrast to #313, the frequency of Tax-specific CD8$^+$ T-cells in #287 decreased from 1.17%

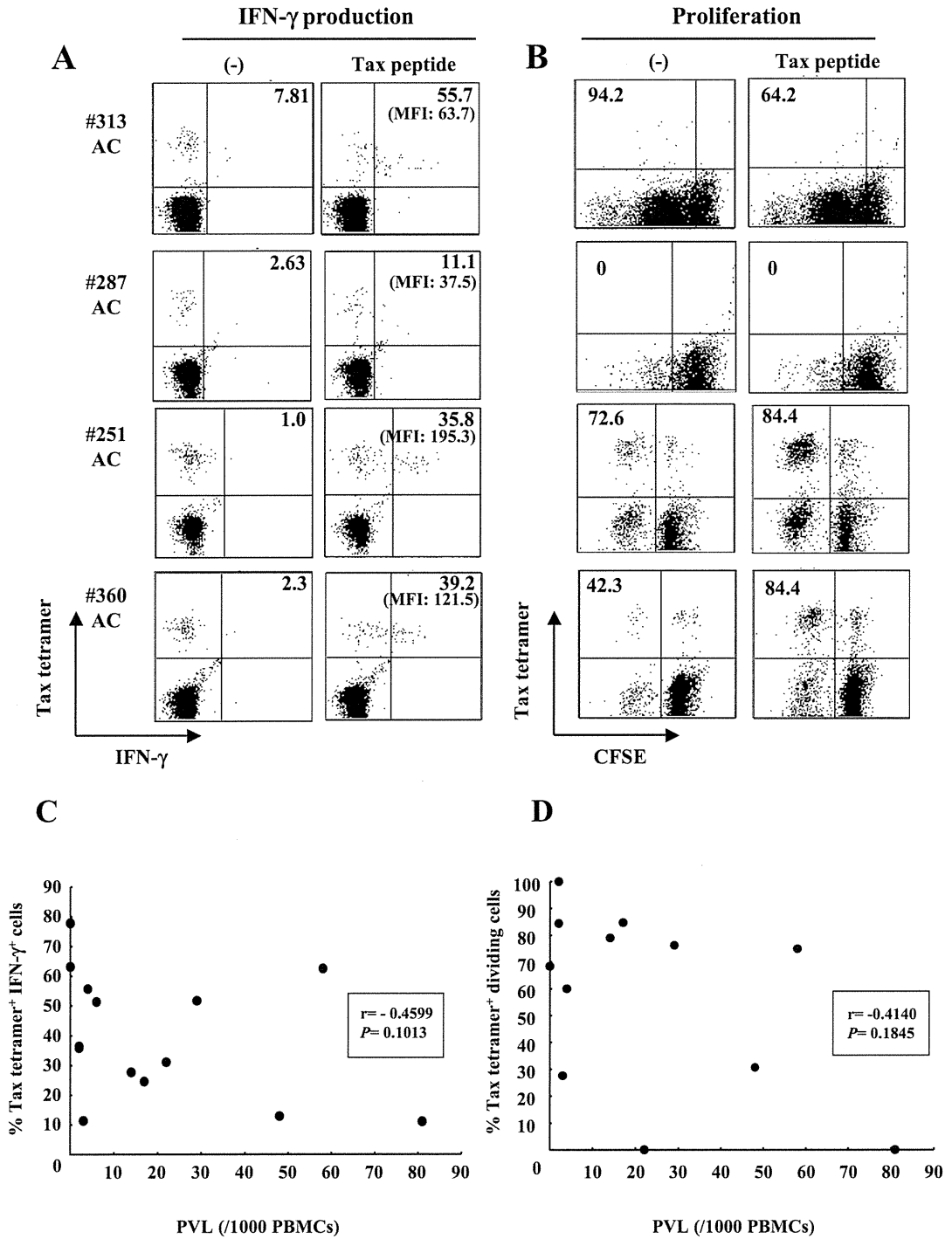

Figure 3 IFN-γ production and cell proliferation of Tax-specific CD8$^+$ T-cells in ACs. (A, B) IFN-γ production (A) and cell proliferation (B) of Tax-specific CD8$^+$ T-cells in PBMCs from 4 ACs were assessed as in Figure 2. The number given in parenthesis shows mean fluorescence intensity (MFI) of IFN-γ expression in the IFN-γ$^+$ tetramer$^+$ cells. (C, D) Relation between the percentage of IFN-γ$^+$ (C) or dividing (D) Tax-specific CD8$^+$ T-cells and proviral loads (PVL) in ACs. Dots represent individual ACs. The Spearman rank correlation test was used to determine correlations and *P* values.

to 0.2% after stimulation with Tax peptide, and was not recovered by LPS stimulation (Figure 4A). In addition, HTLV-1-infected cells have been reported to express C-C chemokine receptor type 4 (CCR4) and have FoxP3$^+$ Treg-like function[18,40]. However, the proliferative ability of Tax-specific CD8$^+$ T-cells in #287 was not restored even in the absence of CCR4$^+$ infected cells (data not shown).

To further examine the function of Tax-specific CD8$^+$ T-cells in #313 and #287, we observed the expression of CD69, an early activation marker transiently expressed on T lymphocytes that precedes cytokine secretion after antigenic stimulation, and CD107a, a marker of degranulation associated with cytotoxic activity in an antigen-specific manner[41]. CD69 was up-regulated on Tax-specific CD8$^+$ T-cells in #313 when stimulated with Tax peptide, but not in #287, which was in agreement with their abilities to produce IFN-γ (Figure 4B). In #313, 22.4% of Tax-specific CD8$^+$ T-cells mobilized CD107a to the surface during a 6-hr culture with Tax peptide stimulation, while CD107a surface expression was detected on 4% of Tax-specific CD8$^+$ T-cells in the culture without stimulation (Figure 4C). However, no CD107a mobilization was detected on the surface of Tax-specific CD8$^+$ T-cells in #287 with or without Tax peptide stimulation (Figure 4C). These results indicate that HTLV-1-specific CD8$^+$ T-cells in AC #287 did not properly activate upon antigen stimulation, and therefore failed to control HTLV-1-infected cells.

The Tax/HLA tetramers used in this study allow us to evaluate the functions of CD8$^+$ T-cells only against an immunodominant epitope, Tax. We therefore compared HTLV-1 Gag p19 in the culture between whole and CD8$^+$ cell-depleted PBMCs to examine the role of total HTLV-1-specific CD8$^+$ T-cells including the dominant Tax-specific CD8$^+$ T-cells, in suppression of HTLV-1 production from infected cells (Figure 4D). As expected, depletion of CD8$^+$ cells from PBMCs in #313 led to significantly higher HTLV-1 production compared to whole PBMCs (P = 0.0115). In contrast, HTLV-1 p19 production increased only a little in the culture of CD8$^+$ cell-depleted PBMCs in #287 (P = 0.1563), indicating that HTLV-1-specific CD8$^+$ T-cells other than the dominant Tax-specific CD8$^+$ T-cells might have a reduced ability to control the infected cells in this donor. It is of note that HTLV-1-infected cells from both two donors carried intact HTLV-1 proviral genomic DNA because HTLV-1 p19 could be detected after 7 day-culture.

Phenotypic analysis of functional and dysfunctional Tax-specific CD8$^+$ T-cells

We next characterized the differentiation status of memory T-cells in Tax-specific CD8$^+$ T-cells. Human CD8 T-cells may be classified as naïve T-cells (CD45RA$^+$CCR7$^+$CD27$^+$), T_{CM} (CD45RA$^-$CCR7$^+$CD27$^+$), T_{EM} (CD45RA$^-$CCR7$^-$CD27$^+$), and T_{Diff} (CD45RA$^+$CCR7$^-$CD27$^-$) cells[42-44]. As shown in Figure 5A, almost all Tax-specific CD8$^+$ T-cells in both #313 and #287 were skewed to CD45RA$^-$CCR7$^-$CD27$^+$ T_{EM} cells, and there was no essential difference between two donors.

A previous report has shown that PD-1 was highly up-regulated on Tax-specific CD8$^+$ T-cells in ATL patients and ACs[32]. We therefore examined PD-1 expression on Tax-specific CD8$^+$ T-cells in several AC samples, including #287. The frequency of PD-1$^+$ Tax-specific CD8$^+$ T-cells was very high in #309 (85.3%) and #313 (96%) (Figure 5B and Table 2) while those Tax-specific CD8$^+$ T-cells retained the proliferative and the cytokine-producing abilities (Figure 3A and Table 2). In #287, the frequency of PD-1-expressing Tax-specific CD8$^+$ T-cells (55.6%) was lower than #309 and #313, but higher than that of PD-1$^+$ CMVpp65-specific CD8$^+$ T-cells in the same donor (Figure 5B). The levels of PD-1 expression showed a similar tendency to the frequency of PD-1$^+$ T-cells. In addition, the blockade of PD-1/PD-ligand 1 (PD-L1) pathway did not restore the proliferative capacity of Tax-specific CD8$^+$ T-cells in #287 (data not shown).

Conserved functions of CMV-specific CD8$^+$ T-cells in #287

We next examined whether the impairment of proliferative capacity and effector functions observed in #287 CD8$^+$ T-cells were specific for HTLV-1 antigens or the result of general immune suppression. PBMC from #287 contained CMVpp65-specific CD8$^+$ T-cells (2.3% of CD8$^+$ T-cells), as detected by tetramer staining. The frequency of CMVpp65-specific CD8$^+$ T-cells increased from 2.3% to 66.0% following in vitro CMVpp65 peptide stimulation, but not without the peptide stimulation (Figure 6A). Antigen-specific IFN-γ and CD69 expression were clearly detected in CMVpp65-specific CD8$^+$ T-cells in #287 (Figures 6B and 6C). Furthermore, CMVpp65-specific CD8$^+$ T-cells mobilized CD107a to the surface in response to CMVpp65 peptide (Figure 6D). These results demonstrate that in #287, CMVpp65-specific CD8$^+$ T-cells, but not Tax-specific CD8$^+$ T-cells, have proliferative potential and effector functions, such as cytotoxic activity and IFN-γ release, suggesting that the impaired CD8$^+$ T-cell function in #287 was specific for HTLV-1.

Dysfunction of Tax-specific but not CMVpp65-specific CD8$^+$ T-cells also in sATL patients

Finally, we extended the study to see whether patients with early stage ATL might exhibit similar dysfunction selective for HTLV-1-specific CD8$^+$ T-cells. We found two smoldering ATL (sATL) patients (#110 and #353)

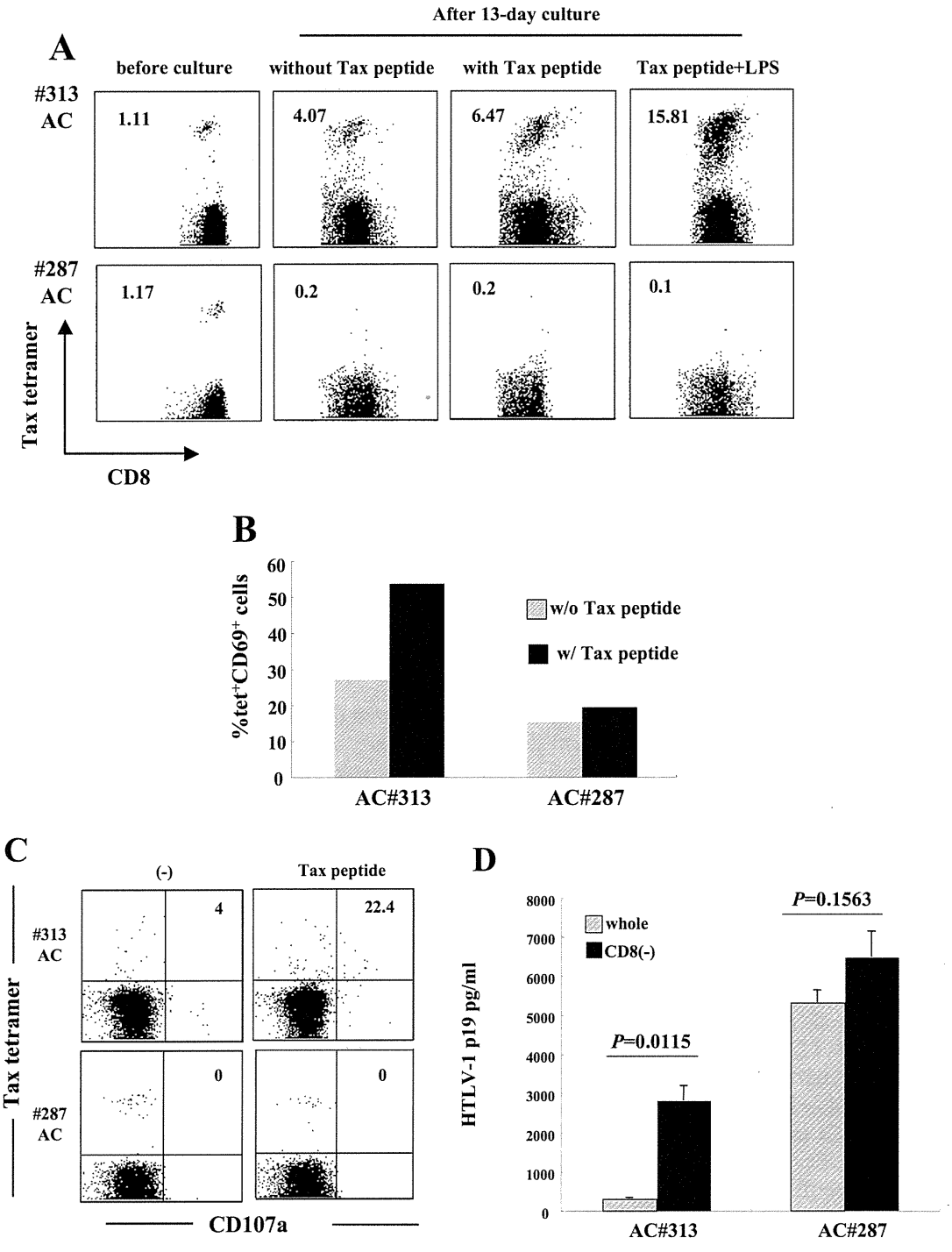

Figure 4 Dysfunction of Tax-specific CD8$^+$ T-cells and inefficient CD8$^+$ cell-mediated HTLV-1 control in AC#287. (A) For antigen-specific T-cell proliferation, PBMCs from #313 and #287 were cultured for 13 days with or without Tax peptide in the presence or absence of 0.1 μg/ml LPS. The number indicates the percentage of tetramer$^+$ cells in CD8$^+$ T-cells. (B, C) PBMCs were stimulated with or without 10 μM Tax peptide for 6 hrs. The expression of CD69 (B) and CD107a (C) in Tax-specific CD8$^+$ T-cells was analyzed by flow cytometry. (B) Bar indicates the percentage of CD69$^+$ cells in Tax-specific CD8$^+$ T-cells. (C) The number represents the percentage of CD107a$^+$ cells in Tax-specific CD8$^+$ T-cells. (D) Whole PBMCs and CD8-depleted fractions in ACs (#287 and #313) were cultured for 7 days and HTLV-1 p19 in the supernatants were measured by HTLV-1 p19 ELISA. *P* value was determined by the unpaired *t* test.

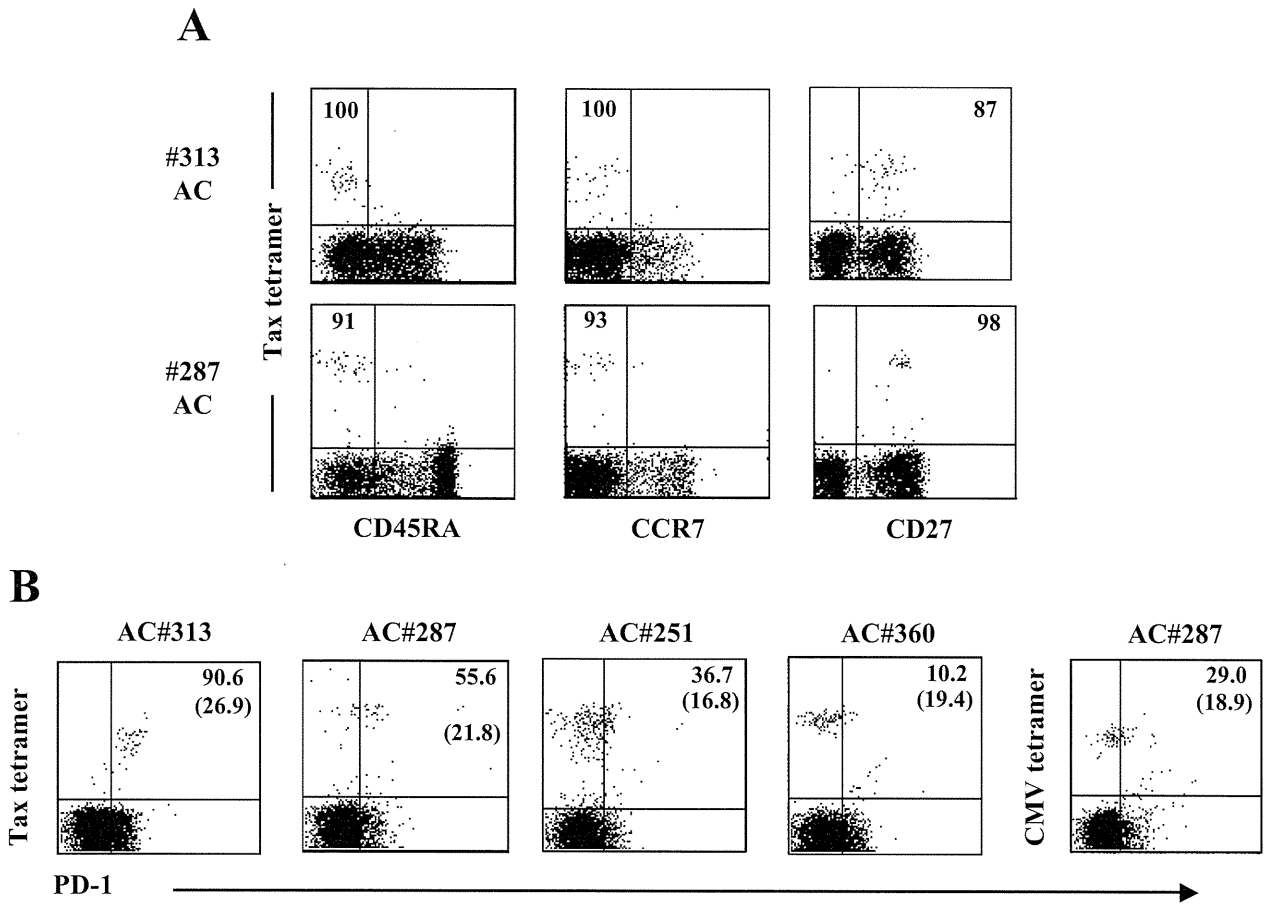

Figure 5 Phenotypic analysis of functional and dysfunctional Tax-specific CD8$^+$ T-cells. (A) Differentiation memory phenotype, based on the expression of CD45RA, CCR7, and CD27 and (B) PD-1 expression of Tax-specific CD8$^+$ T-cells from ACs were examined by flow cytometry. The number represents the percentage of indicated marker-positive or -negative cells in tetramer$^+$ CD8$^+$ T-cells. The number given in parenthesis shows MFI of PD-1 expression on the PD-1$^+$ tetramer$^+$ cells.

possessing 6.89% and 3.15% of tetramer-binding Tax-specific CD8$^+$ T-cells, respectively. The sATL patient #353 carried 5% of abnormal lymphocytes (ably) with a normal range of lymphocyte number, whose status is very close to the borderline with ACs. Patient #110 carried 4% of abnormal lymphocytes with mild lymphocytosis. Tax-specific CD8$^+$ T-cells of two sATL patients (#110 and #353) did not proliferate in response to Tax peptides as similarly observed in a cATL patient (#224) (Figure 7A) and most other cATL patients (Figure 2A and Additional file 1). In contrast, CMVpp65-specific CD8$^+$ T-cells in both sATL patients vigorously proliferated when stimulated with CMVpp65 peptides. CMVpp65-specific CD8$^+$ T-cells in a cATL (#224) also proliferated, but to a lesser degree, which might reflect general immune suppression in this patient (Figure 7).

Discussion

In this study, we detected Tax-specific CD8$^+$ T-cells in 87%, but not the rest of ACs tested, by using tetramers containing Tax major epitope-peptides presented by HLA-A*0201, A*1101, and A*2402. Tax-specific CD8$^+$ T-cells were also detected in 38% of cATL patients, but at reduced frequencies and with severely impaired functions. Further analysis of Tax-specific CD8$^+$ T-cells in 14 ACs indicated that they were functional in most of ACs tested except one (#287), whose Tax-specific CD8$^+$ T-cells poorly responded to specific peptides. However, CMVpp65-specific CD8$^+$ T-cells of this individual were fully functional. Similar T-cell dysfunction selective for HTLV-1, but not CMV, was also observed in sATL patients, one of which (#353) had no clinical symptoms but 5% abnormal lymphocytes. General immune suppression might partly account for the scarcity and/or the dysfunction of Tax-specific CD8$^+$ T-cells in ATL patients, but not those in the AC or the sATL patients as they were selective for HTLV-1. These findings suggest that HTLV-1-specific immune suppression is undergoing in a minor group of ACs and an early stage of ATL.

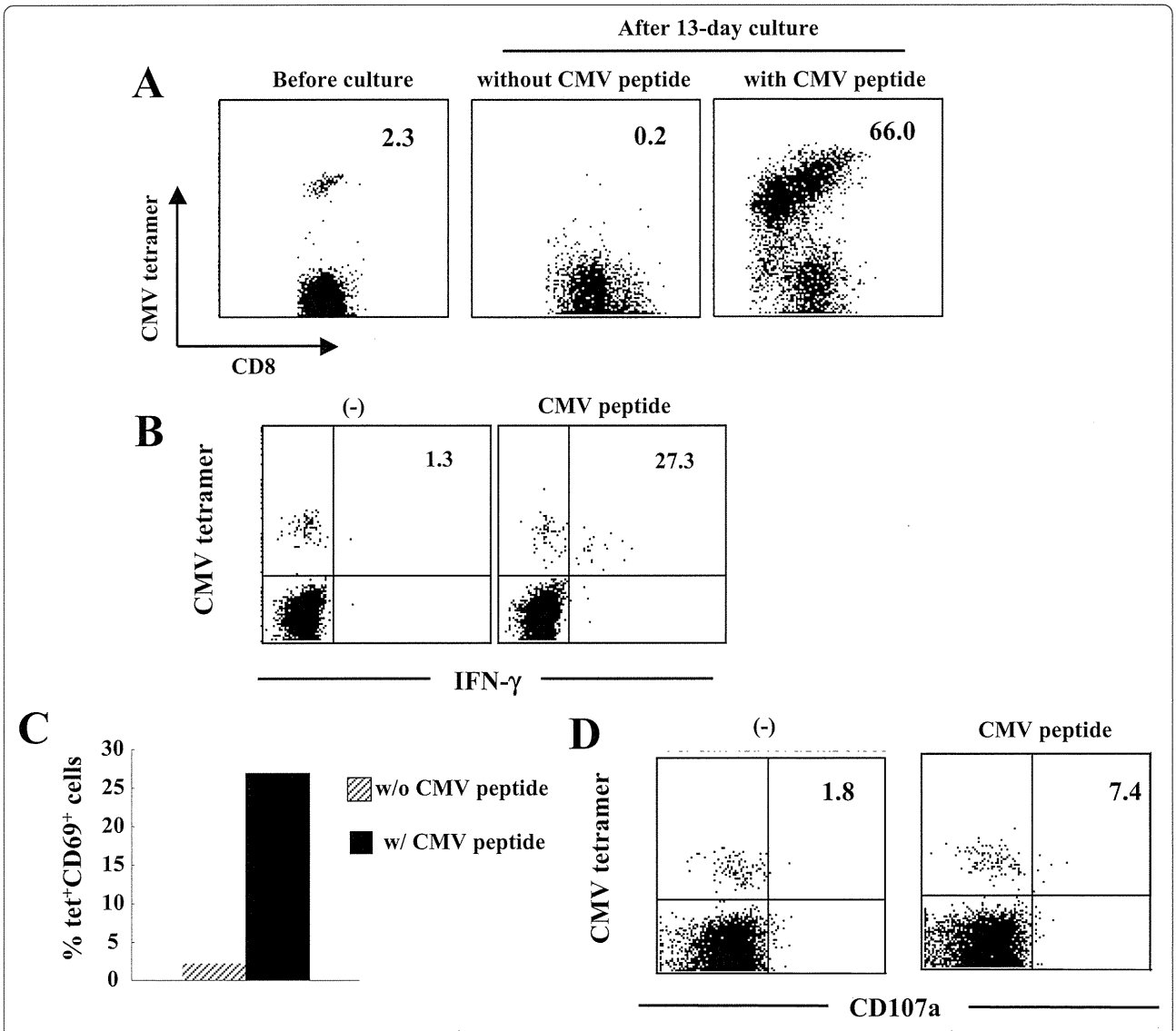

Figure 6 Conserved functions of CMV-specific CD8$^+$ T-cells in AC#287. (A) For antigen-specific T-cell proliferation, PBMCs from #287 were cultured for 13 days with or without 100 nM CMV peptide. The number indicates the percentage of CMV tetramer$^+$ cells in CD8$^+$ T-cells. (B-D) PBMCs were stimulated with or without 10 μM CMV peptide for 6 hrs. IFN-γ production (B), CD69 (C) and CD107a (D) expression of CMVpp65-specific CD8$^+$ T-cells in #287 was analyzed by flow cytometry. (B, D) The number represents the percentage of the indicated marker-positive cells in CMVpp65-specific CD8$^+$ T-cells. (C) Bar indicates the percentage of CD69$^+$ cells in CMV-specific CD8$^+$ T-cells.

The presence of tetramer-binding Tax-specific CD8$^+$ T-cells in cATL patients, although at low frequencies, implies that they have encountered antigen during the chronic phase of ATL disease, suggesting that Tax may be expressed *in vivo*. This may be supported by a previous report showing that virus-specific CD8$^+$ T-cells fails to acquire memory T-cell property of long-term antigen-independent persistence during chronic lymphocytic choriomeningitis virus (LCMV) infection[45]. However, there is no direct evidence that infected cells produce Tax in infected individuals. HTLV-1-specific T-cell responses in cATL patients are largely different from HAM/TSP patients. In HAM/TSP patients, Tax-specific CD8$^+$ T-cells proliferated vigorously and a large population of them produced IFN-γ. In contrast, the function of Tax-specific CD8$^+$ T-cells in cATL patients was profoundly suppressed, similarly to tumor infiltrating lymphocytes (TIL)[46]. In cATL patients, Tax-specific CD8$^+$ T-cells that were detected before culture decreased in number to undetectable or very low levels after 6 days, regardless of peptide stimulation (data not shown). This is not likely to be due to TCR down-regulation, because TCRs on Tax-specific CD8$^+$ T-cells in HAM/TSP patients are down-regulated on days 1 to 4

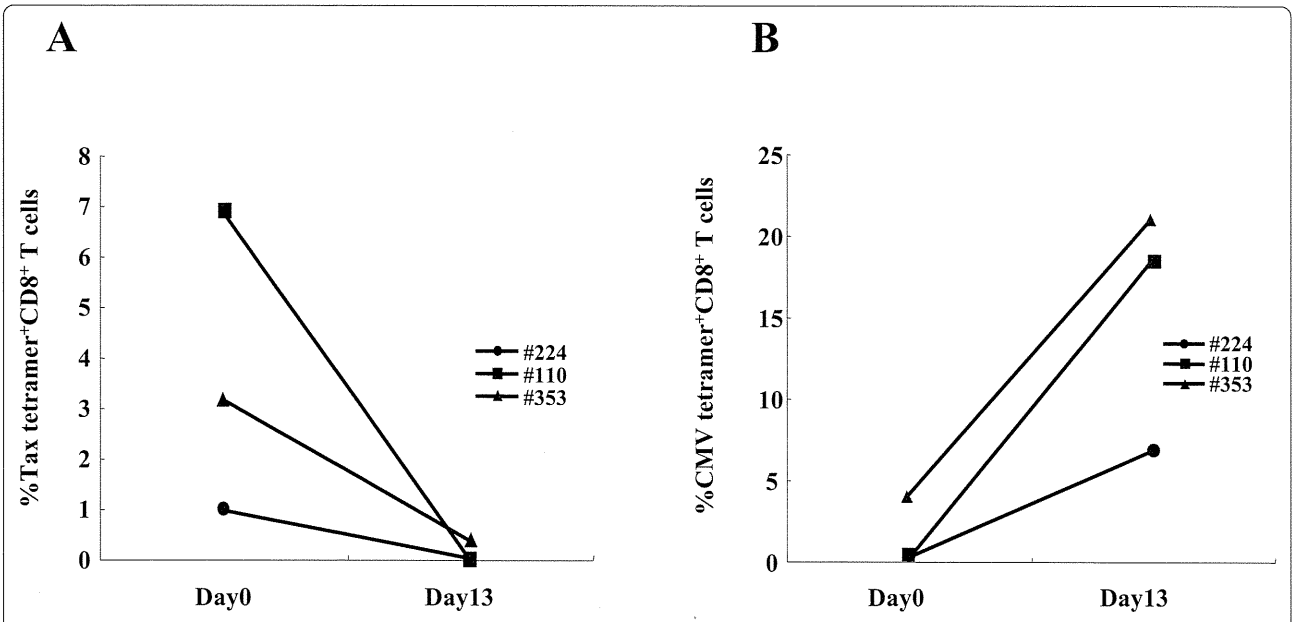

Figure 7 Impaired proliferation of Tax-specific but not CMVpp65-specific CD8$^+$ T-cells in sATL patients. For antigen-specific T-cell proliferation, PBMCs from sATL (#110; square, #353; triangle) and cATL (#224; circle) patients were cultured for 13 days with 100 nM Tax (A) or CMV (B) peptide. Each dot indicates the percentage of tetramer$^+$ cells in CD8$^+$ T-cells at day 0 and day 13 after culture. Clinical information on ATL patients used here is as follows; sATL#110: age; 40 s, gender; F, WBC#; 11,000/μL {lymphocyte (lym); 39%, abnormal lymphocytes (ably); 4%}, cATL#224: age; 50 s, gender; F, WBC#; 7900/μL (lym; 30%, ably; 33%), sATL#353: age; 60 s, gender; M, WBC#; 4620/μL (lym; 39%, ably; 5%).

and reappeared by day 6 in vitro[34]. Moreover, we could not observe any tetramer$^+$ CD8$^+$ T-cells even in the 13-day culture (data not shown), suggesting these cells might have died during the culture.

Severe dysfunction of Tax-specific CD8$^+$ T-cells was observed not only in cATL patients, but also in an AC #287. Fresh PBMCs of #287 contained 1.17% tetramer$^+$ cells in the CD8$^+$ T-cell fraction. However, none of these tetramer-positive T-cells proliferated in culture, with or without Tax peptide stimulation (Figure 3B). Although a few populations of them (11.1%) produced a small amount of IFN-γ, they lacked degranulation activity for cytotoxicity or expression of CD69, an early activation marker, upon specific stimulation (Figures 3 and 4). Importantly, CMVpp65-specific CD8$^+$ T-cells in the same donor were clearly activated, and exhibited these characteristics upon stimulation with pp65 peptides (Figure 6). These observations indicated that the impaired Tax-specific CD8$^+$ T-cells function in #287 was not attributable to general immune suppression, but to an HTLV-1-specific phenomenon. In addition, CD8-depletion study indicated that not only the dominant Tax-specific CD8$^+$ T-cell function but also other HTLV-1-specific CD8$^+$ T cell responses might be reduced in #287 (Figure 4D). Since CMV-specific CD8$^+$ T-cells responded well to the specific peptides, antigen-presenting cells in culture were not likely to be responsible for the selective suppression of Tax-specific CD8$^+$ T-cells. In addition, it has been shown that HTLV-1-infected cells generally express CCR4 and have Treg-like function[18,40]. However, depletion of CCR4$^+$ cells did not restore the proliferative ability of Tax-specific CD8$^+$ T-cells (data not shown), indicating that suppression of the infected cells were not likely to be the major reason for the impaired Tax-specific CD8$^+$ T-cell function in our culture system. These observations suggest that in #287, Tax-specific CD8$^+$ T-cells themselves might lose their functions.

Many chronic viral infections affect the phenotype, function, and maintenance of memory T-cells [24,42,47,48]. T_{EM} cells predominate in infections in which relatively high levels of antigen persist and continuous antigen stimulation are required for maintenance of T_{EM} cells. As described in HAM/TSP patients [34], Tax-specific CD8$^+$ T-cells in both ACs (#287 and #313) were primarily enriched in T_{EM} memory pool in spite of the functionality of Tax-specific CD8$^+$ T-cells (Figure 5A), which may support continuous or periodical expression of viral antigen in vivo during an asymptomatic stage.

PD-1 is known to play a major role in regulating T-cell exhaustion during chronic infection. In this study, we could not obtain any data supporting the involvement of PD-1 in the dysfunction of Tax-specific CD8$^+$ T-cells. However, we observed that Tax-specific CD8$^+$ T-cells in some ACs showed IFN-γ production, but not

proliferative capacity (Table 2). This partially lacked function of Tax-specific CD8$^+$ T-cells is similar to the features of T-cell exhaustion. Whether Tax-specific CD8$^+$ T-cells are exhausted in HTLV-1 infection, and whether other molecules associated with T-cell exhaustion are involved in the impairment of Tax-specific CD8$^+$ T-cell responses are necessary to be clarified because some inhibitory molecules such as T-cell immunoglobulin and mucin domain-containing protein-3 (TIM-3), lymphocyte activated gene-3 (LAG-3), and transcription factors including BLIMP-1 are also found to be associated with T-cell exhaustion [49].

The incidence of Tax-specific CD8$^+$ T-cell detection was high (87.0%) in ACs. Given the fact that the incidence of Tax-specific CD8$^+$ T-cells in HAM/TSP patients was 100%, a small fraction of ACs lacking detectable tetramer-binding cells might lack Tax-specific T-cell responses. Our previous study investigating GST-Tax protein-based T-cell responses supports this notion [20]. In the present study, even in ACs possessing Tax-specific CD8$^+$ T-cells, at least one individual exhibited T-cell dysfunction selectively for HTLV-1. The incidence of tetramer-positive cells was reduced in ATL patients (38.1%), and the function of these cells was impaired in all the ATL patients even with detectable tetramer-binding Tax-specific CD8$^+$ T-cells. Our findings suggest that HTLV-1-specific T-cell responses are selectively impaired in a small percentage of HTLV-1-infected individuals in the asymptomatic stages, and the proportion of individuals with such characteristics increase as the stages proceed towards ATL. Strategies to reactivate HTLV-1-specific T-cells at early stages might contribute to a reduction in the immunological risk of ATL.

Conclusions

Tax-specific CD8$^+$ T-cells were scarce and dysfunctional in a limited AC population and ATL patients, and the dysfunction of CD8$^+$ T-cells was selective for HTLV-1 in early stages. These results implied the presence of some HTLV-1-specific T-cell suppressive mechanisms even in asymptomatic stages, which are not a result of general immune suppression in ATL but could be underlying conditions toward disease progression.

Methods

Samples

Blood samples from 64 HTLV-1-seropositive individuals were used in this study: 23 asymptomatic carriers (ACs), 18 HAM/TSP patients, 2 smoldering type ATL (sATL) patients, and 21 chronic type ATL (cATL) patients. All blood samples were obtained following written informed consent, and this study was reviewed and approved by the Institutional Review Board of the Tokyo Medical and Dental University.

Peptides

Peptides used in this study were HLA-A2-restricted CTL epitopes (Tax11-19, LLFGYPVYV)[12] (Hokudo Co., Hokkaido, Japan) and (CMV495-503, NLVPMVATV)[50] (Sigma Aldrich St. Louis, MO), HLA-A11-restricted CTL epitope (Tax88-96, KVLTPPITH)[36] (Hokudo Co) and HLA-A24-restricted CTLs epitopes (Tax301-309, SFHSLHLF)[35] (Hokudo Co) and (CMV341-349, QYDPVAALF)[51] (Sigma Aldrich).

Cell Surface staining

To select samples carrying HLA-A2, -A11, or -A24, whole blood was screened with antibodies for HLA-A2, -A11, and -A24 subtypes (One Lambda, Inc., Los Angeles, CA). FITC-conjugated goat anti-mouse Ig (G+M) (Beckman Coulter Inc., Webster, TX) was used as a secondary antibody. For cell surface staining, whole blood samples were stained with the following fluorochrome-conjugated mouse anti-human mAbs; CD3-FITC, CD8-PE/Cy5, CD8-PerCP/Cy5.5 (RPA-T8, BioLegend), CD27-FITC (O323, BioLegend) CD45RA-FITC (HI 100, BD Biosciences), CD45RA-APC (HI 100, BioLegend), CD69-FITC (FN 50, BioLegend), PD-1-FITC (EH12.2H7, BioLegend), CCR7 (TG8/CCR7, Biolegend).

Tetramer staining

PE-conjugated HLA-A*0201/Tax11-19, HLA-A*1101/Tax88-96, HLA-A*2402/Tax301-309, HLA-A*0201/CMVpp65, HLA-A*2402/CMVpp65 tetramers were purchased from MBL (Nagoya, Japan). Whole blood samples or peripheral blood mononuclear cells (PBMCs) were stained with PE-conjugated Tax/HLA tetramer in conjunction with FITC-conjugated anti-CD3 (UCHT1, BioLegend San Diego, CA), and PE-Cy5-conjugated anti-CD8 monoclonal antibodies (mAbs) (HIT8a, BD Biosciences San Jose, CA). Whole blood samples were lysed and fixed in BD FACS lysing solution (BD Biosciences) before washing the cells. Samples were analyzed on a FACSCalibur (Becton Dickinson, San Jose, CA) and data analyses were performed using CellQuest software (Becton Dickinson).

Tetramer-based IFN-γ flow cytometry

Tetramer-based intracellular IFN-γ flow cytometry was performed as described previously[17], with slight modifications. In brief, PBMCs (2.0×10^5 cells) were incubated with HLA tetramer-PE and anti-CD8-PE/Cy5, washed, and stimulated with 10 μM antigenic peptide for 6 hrs at 37°C in the presence of brefeldin A (BFA, 10 μg/ml; Sigma Aldrich). The cells were stained with a